diversity

MDPI

Article

An Empirical Framework for Testing the Stress–Dominance Hypothesis: Two Adversity Gradients, Three Trait Components, and Spatial Scale

Hanna Tutova [1], Olena Lisovets [2], Olha Kunakh [2,*], Anastasiia Zymaroieva [1,3], Jens-Christian Svenning [3] and Olexander Zhukov [2]

[1] Department of Botany, Ecology and Horticulture, Bogdan Khmelnytskyi Melitopol State Pedagogical University, 72300 Zaporizhzhia, Ukraine; annatutova37@gmail.com (H.T.); zymaroieva@bio.au.dk or nastya.zymaroeva@gmail.com (A.Z.)
[2] Department of Biodiversity and Ecology, Oles Honchar Dnipro National University, Gagarin av., 72, 49000 Dnipro, Ukraine; lisovetselena@gmail.com (O.L.); zhukov_dnipro@ukr.net (O.Z.)
[3] Centre for Ecological Dynamics in a Novel Biosphere (ECONOVO), Department of Biology, Aarhus University, Ny Munkegade 114, DK-8000 Aarhus C, Denmark; svenning@bio.au.dk
* Correspondence: kunah_olga@ukr.net

Abstract

The Stress–Dominance Hypothesis predicts changes in functional trait dispersion along gradients of environmental and competitive adversity. However, empirical testing is complicated by issues such as null-model specification, overlapping ecological functions of traits, and the identification of adversity gradients. An empirical framework for testing these predictions in aquatic macrophyte communities was applied, combining null-model randomisation with an orthogonal decomposition of the species-by-traits matrix into environment-sensitive, competition-sensitive, and residual components. The framework was tested using data from 453 sampling locations in the Dnipro–Orilskyi Nature Reserve (Ukraine), where 100 aquatic macrophyte species were recorded during four sampling campaigns conducted from May to August 2024. Environmental and competitive adversity were quantified using indicators derived from community-level plant strategy composition. High environmental adversity was associated with underdispersion of environment-sensitive traits, consistent with environmental filtering, and this pattern was predominantly structured at broad spatial scales. Conversely, high competitive adversity was associated with overdispersion of competition-sensitive traits, consistent with limiting similarity under symmetric competition, with a greater contribution from finer spatial scales. Competition also generated an alternative pattern: trait convergence associated with asymmetric competition was detected in the residual trait component and exhibited substantial medium- and fine-scale structure. These results indicate that environmental and competitive adversity represent distinct dimensions of community assembly, and that their effects on functional diversity can be distinguished by combining trait decomposition, appropriate null models, and spatial information.

Keywords: trait dispersion; environmental filtering; limiting similarity; null models; trait-matrix

Check for updates

Academic Editors: Dubravka Špoljarić Maronić, Filip Stević, Tanja Žuna Pfeiffer and Anita Galir

Received: 4 September 2026
Revised: 12 November 2026
Accepted: 16 November 2026
Published: 18 November 2026

Copyright: © 2026 by the authors. Licensee MDPI, Basel, Switzerland. This article is an open access article distributed under the terms and conditions of the Creative Commons Attribution (CC BY) license.

1. Introduction

Functional diversity indices provide a basis for evaluating alternative ecological assembly rules by identifying deviations of the observed community structure in trait space from

null expectations and relating these deviations to different underlying assembly processes, such as niche-based filtering, limiting similarity, or neutral assembly [1]. These processes are expected to generate different patterns of functional trait dispersion within communities. In particular, niche-based filtering constrains local community membership by favouring species whose functional traits are compatible with local abiotic conditions [2]. As a consequence, co-occurring species may become more functionally similar than expected under random assembly, producing trait convergence and functional underdispersion [3]. An alternative assembly process is interspecific competition, which can promote limiting similarity among coexisting species [4]. Limiting similarity leads to trait divergence, which, at the level of functional diversity, is expressed as functional overdispersion relative to null expectations by favouring differentiation in resource-use traits [5]. Functional convergence can be induced by competition when species with traits conferring higher competitive ability exclude weaker competitors [6–8]. Such exclusion is expected under asymmetric competition [9]. Discriminating among alternative ecological assembly rules using functional diversity indices requires an explicit null-model framework, as inference depends on the constraints imposed during randomisation, including species-pool definition, habitat stratification, and spatial scale [10].

The patterns of biodiversity are understood to be closely linked to ecological assembly rules, which vary across spatial scales [11] and environmental gradients [12]. The qualitative model for trait dispersion [13], later termed the Stress-Dominance Hypothesis (SDH) by Swenson & Enquist [14], delineates the resource-constraint gradients along which different traits' dispersion patterns predominate, interpreted in terms of environmental versus competitive adversity [13]. The SDH states that as the environment becomes more stressful, stabilising selection will increasingly limit ecological and evolutionary variation in plant function within a community [14]. Stress refers to constraints on a community that limit the rate of resource acquisition, growth, or reproduction of organisms [13,15]. External stressors, such as abiotic factors like drought or salinity, as well as disturbances caused by fire, runoff, or predation, generate environmental adversity. Traits associated with overcoming environmental adversity tend to be underdispersed, reflecting strong environmental filtering. In contrast, traits associated with coping with competitive adversity tend to be overdispersed in environments where resources or space are limited by internal community constraints, such as interspecific competition [13]. In their original conceptual framework, Weiher and Keddy [13] distinguished between environmental and competitive adversity but represented them along a single gradient for simplicity, an assumption that may lead to misunderstandings. The authors explicitly acknowledged that these two gradients could be considered separately and identified the spatial scale of investigation as an additional dimension of community assembly. Overdispersion is expected mainly at small spatial scales, where competitive adversity predominates, whereas underdispersion tends to occur at broader spatial scales, where environmental adversity is more important [13]. The original conceptual model of the SDH, termed "A qualitative model for trait dispersion" by Weiher and Keddy (1995) [13], also identifies an intermediate zone between underdispersion and overdispersion, characterised by randomness, historical effects, and chaos. In this zone, community assembly patterns may depend strongly on historical contingencies, such as the sequence of species colonisation, rather than exhibiting consistent trait convergence or divergence [16].

Ecological assembly rules affect traits differentially. Accordingly, the predictions of the Stress-Dominance Hypothesis (SDH) pertain to distinct groups of traits [17]. The typology of traits includes four categories: stress-tolerance traits, competitive dominance traits, niche-differentiation/resource-use traits, and trade-off traits [18]. Stress-tolerance traits enable survival under high abiotic stress. Under strong stress, environmental filtering reduces func-

tional diversity through trait convergence. Competitive dominance traits confer advantages in competitive interactions and are filtered under high competition, which likewise results in convergence and reduced functional diversity. This pattern corresponds to the "convergent for the competition trait under asymmetric competition" scenario described by Götzenberger et al. [9]. Niche-differentiation/resource-use traits facilitate coexistence by reducing niche overlap. In stressful environments, functional diversity in these traits decreases due to environmental filtering, whereas increased competition promotes divergence, thereby increasing diversity [18]. Lopez et al. [19] consider a trait typology comprising "alpha traits" and "beta traits," which correspond, respectively, to the alpha and beta niches [20]. Functional traits are commonly classified according to their presumed associations with environmental filtering or competition [21]. In the vast majority of cases, a particular trait provides multiple functions and is involved in the plant's adaptation to environmental factors and in its ability to persist under competition [22]. This challenge highlights the potential of high-dimensional trait approaches that summarise multiple traits into a small set of (approximately) orthogonal composite axes describing the major dimensions of phenotypic and niche differentiation [23]. By collapsing complex multivariate trait spaces into a few orthogonal axes, these methods facilitate visualisation and analysis of functional strategies and provide a compact representation of the gradients along which multiple ecological processes may act [24]. In such frameworks, multivariate analyses (e.g., PCA) can be used to derive orthogonal axes that correspond to α- and β-niche dimensions, that is, traits primarily sensitive to competition and to environmental gradients, respectively [25].

Some studies support the predictions of the SDH [14,26,27] or provide partial support [28], whereas many others report substantial deviations from SDH-based expectations [18,29–32]. Several potential sources of these conflicting outcomes have been identified [17]. Differences in the test statistics employed [33] and in the choice of null model [9] can yield contradictory conclusions. Sample size and sampling extent also affect the apparent form of the relationship [34]. Reducing the two adversity axes to a single dimension can lead to instances in which empirical support for the SDH is misinterpreted as evidence against it [35]. Ambiguity in the definition of "stress" may confound hypothesis testing. Treating stress as the effect of an external factor leads to an oversimplification, whereby qualitatively different drivers are assumed to be equivalent, which is not the case. Under this interpretation, external constraints correspond more closely to stressors than to stress itself. Conceptually, it is therefore more appropriate to interpret stress as the biological system's response to adverse environmental conditions (i.e., to environmental stressors). As defined by H. Selye: "In the biological sense, stress is the interaction between damage and defence, just as in physics tension or pressure represents the interplay between a force and the resistance offered to it" [36]. Under this interpretation, responses to different levels of environmental factors (stressors) may be broadly similar, consistent with the nonspecific nature of the stress response [37]. Given that stress measured from the 'plant's eye view' is relative to a particular species [38], the resulting outcomes of biotic interactions along stress gradients may vary depending on the stress tolerance and competitive ability of the species involved [39–41]. Clearly, defining a stress gradient in terms of ecosystem response, rather than solely in terms of external constraints, may improve the correspondence between the hypothesis's predictions and empirical results. However, defining a stress gradient in terms of ecosystem response implies using community-based indicators rather than directly measured external factors; that is, employing phytoindication to quantify the community's stress level. Community biomass has been proposed as a proxy for community-level stress [30], whereas NDVI provides an analogous indicator at broader geographic scales [17]. Moreover, applying the CSR model at the community level to quantify a community's functional signature [42] has been shown in multiple case studies to predict community responses

to stress and disturbance with good accuracy [43–45]. Quantifying stress and competitive intensity is essential for estimating environmental and competitive adversity, both of which are crucial for testing the Stress–Dominance Hypothesis.

The relative importance of assembly processes that generate trait convergence or divergence along adversity gradients varies with the spatial scale considered [13]. Spatially explicit sampling is essential because it reveals whether co-occurring species are aggregated or segregated at fine scales across a stress gradient, allowing one to infer when microenvironmental filtering or facilitation versus competitive exclusion dominates community assembly [46]. Fine-scale spatial information is critically important for successfully inferring assembly rules along stress gradients. This is because shifts in species co-occurrence from segregation to aggregation, along with the scale dependence of these patterns, are key factors in distinguishing interaction-driven structuring (competition versus facilitation) from microenvironmental filtering [47]. Trait assembly patterns are spatially scale-dependent. At fine spatial grains, co-occurring species more often exhibit trait divergence, promoting coexistence via niche differentiation consistent with limiting similarity. At medium and broad spatial scales, trait convergence is more frequently observed, reflecting environmental filtering. At the landscape scale, departures from random expectations often diminish because filtering signals can be obscured by dispersal limitation [48]. These findings underscore the importance of explicitly accounting for spatial scale, as predicted by the Stress–Dominance Hypothesis (SDH).

Testing the Stress–Dominance Hypothesis requires accounting for its proposition of two alternative adversity gradients, within which certain trait groups may either deviate from a random (null) distribution or, conversely, show no such deviation. Traits associated with overcoming environmental adversity are expected to exhibit underdispersion at the extreme values of the environmental gradient, hereafter referred to as environmental adversity. This pattern is predicted to manifest primarily at broad spatial scales. In contrast, traits linked to addressing competitive adversity are expected to exhibit overdispersion at the extreme values of the competitive gradient, hereafter referred to as competitive adversity. This pattern is predicted to manifest primarily at fine spatial scales. Outside these adversity domains, both environment-sensitive and competition-sensitive traits, along with others, are expected to be randomly distributed or to display other deviations from randomness driven by additional community assembly processes.

The objective of this study was to empirically test the predictions of the Stress–Dominance Hypothesis by adapting a methodological approach previously evaluated through numerical experiments. Specifically, we examined how environmental filtering and interspecific competition generate functional trait convergence or divergence, expressed as trait underdispersion or overdispersion, along environmental and competitive adversity gradients and across spatial scales. To this end, we extended the approach by incorporating alternative randomisation procedures, differentiating the contributions of environmental conditions and competition to functional trait variation, and accounting for spatial-scale dependence. The proposed approach was applied to aquatic macrophyte communities of the Dnipro–Orilskyi Nature Reserve (Ukraine) as an empirical case study.

2. Materials and Methods

2.1. General Analytical Framework for Testing the Stress–Dominance Hypothesis

The framework integrates five analytical components: (1) null-model randomisation to identify departures from random trait dispersion; (2) decomposition of the species-by-traits matrix into environment-sensitive, competition-sensitive, and residual components; (3) quantification of environmental and competitive adversity using community-level plant strategy composition; (4) statistical modelling of trait dispersion along the result-

ing adversity gradients; and (5) spatial decomposition of trait dispersion patterns across multiple scales.

Functional diversity was quantified using Rao's quadratic entropy (Rao's Q) [49], calculated from species relative abundances and pairwise functional trait distances. Ten null models were considered to assess statistical power and Type I error rates. Five models represent different ways of randomising the original community matrix (C1–C5), four models involve randomising the species-by-traits matrix (T1–T4), and the range randomisation model combines information from both matrices. In model C1, species' abundances are permuted within each sample among the species present. In C2, species' abundances are permuted within samples across all species, preserving only sample richness and total abundance. In C3, sample abundances are permuted within each species, maintaining each species' occupancy pattern. In C4, sample abundances are permuted among all samples for each species, preserving only the total abundance (frequency) of each species. In C5, species' presences (and associated abundances) are randomised while maintaining sample richness. In T1, entire trait vectors are shuffled among species (all traits together). In T2, each trait is shuffled independently among species. In T3, entire trait vectors are shuffled among species within two abundance classes. In T4, each trait is shuffled independently among species within two abundance classes. In the Range model, species are randomly reassigned within each community from a species pool constrained by the observed ranges of numerical functional traits, while preserving community species richness and the distribution of non-zero species abundances. The R code implementing these randomisation models, together with the original species composition and functional trait matrices required to reproduce the calculations, is publicly available in the Zenodo repository [50].

Comparison of observed Rao's Q values with null-model expectations allows functional convergence and divergence to be identified as patterns of trait underdispersion and overdispersion, respectively. The standardised effect size (SES) for each community was calculated as the deviation of the observed functional diversity from the null-model expectation, scaled by the standard deviation of the null distribution:

$$\mathrm{SES_i} = \frac{Q_i^{\mathrm{obs}} - \mu_i^{\mathrm{null}}}{\sigma_i^{\mathrm{null}}},$$

where Q_i^{obs} denotes the observed functional diversity of the i-th community, μ_i^{null} is the null-model mean, and σ_i^{null} represents the standard deviation of the null-model randomisation distribution. Because the tested null hypotheses were directional, one-sided tests were used, with SES > 1.645 indicating divergence and SES < -1.645 indicating convergence ($\alpha = 0.05$). p-values obtained as the proportion of null-model values more extreme than the observed ones were qualitatively consistent with the SES-based inference.

The power to detect a given assembly scenario is quantified as the proportion of communities correctly classified according to the expected trait pattern. This approach is feasible because functional diversity is typically calculated separately for filtering-related and competition-related traits. Communities generated under a neutral scenario are commonly used to estimate the Type I error rate of a null model, i.e., the probability of detecting one of the focal processes when community assembly is governed solely by drift.

2.2. Adaptation of the Algorithm to Empirical Data

The matrix of functional properties sensitive to environmental factors was obtained as follows. RLQ analysis was employed to identify the dominant joint gradients linking environmental variables, species composition and traits [51]. RLQ yields species scores on axes that maximise the covariance between the environmental matrix and the trait structure. Algebraically, the "ideal" (env-sensitive) traits were computed by regressing the

standardized trait matrix T onto the RLQ species scores Z using species weights W. The weighted normal equations:

$$(Z^\top WZ)\beta = Z^\top WT,$$

were solved using either the matrix inverse or, when necessary, the Moore–Penrose pseudoinverse. Species scores (Z) were obtained as species coordinates on the first two axes of the RLQ analysis, which integrates environmental variables, species composition, and functional traits. Species weights (W) were derived from the correspondence analysis of the community composition matrix and represent the relative contribution of each species to the overall community structure. These weights were subsequently used in the weighted least-squares estimation of the environment-sensitive component of functional traits. The fitted component:

$$T_{\text{env}} = Z\beta$$

which represents the portion of trait variation most strongly associated with the environmental structure captured by the RLQ axes.

The matrix T_{env} was interpreted as the "ideal" environment-sensitive component of species traits, whereas the residual matrix:

$$T_{\text{res}} = T - T_{\text{env}}$$

captures trait variation not explained by the RLQ environment–trait relationship and is used in the competition-related part of the analysis.

The decomposition of trait inertia was quantified by computing the total weighted inertia of the standardized trait matrix (SS_{tot}), the inertia explained by the environment-sensitive component obtained from RLQ (SS_{env}), and the residual inertia (SS_{res}). The proportion $SS_{\text{env}}/SS_{\text{tot}}$ represents the share of total trait inertia that is aligned with the environment–species–trait structure extracted by the RLQ analysis. The RLQ analysis was performed using the ade4 package [52], retaining two RLQ axes for subsequent analyses. Species weights were defined as the column weights obtained from correspondence analysis of the site-by-species community matrix, while site weights were derived from the corresponding row weights. Categorical traits were converted into binary dummy variables, and variables with zero variance were excluded. All quantitative and binary trait variables were subsequently centred and standardised to unit variance, ensuring that differences in their original measurement scales did not directly determine their contributions to the analysis. The same standardisation procedure was applied to the environmental variables.

Estimation of the competition-sensitive trait matrix requires a quantitative representation of species performance under potential competitive interactions. Direct measures of fitness based on survival, growth, or reproductive success were not feasible given the number of species and the number of observations considered here. Therefore, an operational proxy for relative fitness was derived from species positions within ordination space. Canonical correspondence analysis (CCA) was performed using the measured environmental variables as constraints [53]. This procedure partitions variation in species composition into a constrained component explained by the measured environmental variables and an unconstrained residual component. The latter was used to characterise variation in community composition remaining after accounting for the measured environmental gradients. This residual variation may reflect biotic interactions, including competition, but may also contain effects of unmeasured environmental factors and other processes. Within this residual CCA space, species scores defined species-specific reference positions, and the corresponding plot score represented the position of each species occurrence. Ecological mismatch was quantified as the Euclidean distance between each occurrence and the species-specific reference position in the multidimensional ordination space. Smaller

distances were interpreted as indicating higher inferred species performance, whereas larger distances indicated increasing ecological mismatch and, consequently, lower inferred performance. This distance-based measure was used as an operational proxy for species performance rather than a direct measure of demographic or evolutionary fitness. To obtain a standardised and comparable index, distances were transformed using a monotonic decay function:

$$\text{inferred species performance} = \frac{100}{1 + d/s},$$

where (d) is the Euclidean distance between the plot position and the species-specific optimum in the residual CCA ordination space, and (s) is a species-specific scaling constant defined as the 75th percentile of non-zero distances from that optimum. This transformation assigns the maximum inferred species performance (ISP = 100) at the optimum (d = 0) and produces a continuous decline with increasing ecological mismatch. At (d = s), ISP equals 50. Species-specific scaling accounts for differences in the dispersion of species occurrences around their ordination optima, thereby providing a comparable performance index for subsequent estimation of pairwise competition coefficients.

Pairwise interspecific competition coefficients were estimated using the *cxr* package version 1.1.1 [54], which implements likelihood-based competition models parameterised with field co-occurrence and performance data. A pairwise Beverton–Holt (BH) model was fitted for all species simultaneously to estimate the competition coefficient. The analysis included 100 focal species, corresponding to 9900 potential directed interspecific interactions. Model fitting was performed using the BOBYQA optimisation algorithm. The completeness and numerical stability of the resulting interaction matrix were assessed by examining the proportion of finite parameter estimates, missing coefficients, and estimates approaching the predefined parameter bounds. To evaluate the empirical support for individual interaction coefficients, we also calculated the number of co-occurrences for each directed species pair. These diagnostics were used to distinguish the numerical availability of parameter estimates from their observational support, particularly for infrequently co-occurring species. A symmetrised version of the competition matrix was also produced for analyses requiring an undirected representation of competitive interactions, calculated as $(A + A^{\mathsf{T}})/2$. This matrix reflects the average strength of bilateral interactions between species pairs [54]. A singular value decomposition of the directed competition kernel was performed to characterise the structure of interspecific competition [55]. The residual trait matrix (T_res), obtained after removing the environment-sensitive component, was regressed onto a reduced set of leading singular vectors derived from the competition matrix. The fitted values represented the competition-associated component of trait variation (T_bio), whereas the remaining residuals represented trait variation unexplained by the environmental and competition-related components.

Species weights derived from the RLQ framework [56,57] were incorporated into the regressions to account for differences in species representation across the dataset, so that better-represented species contributed proportionally more to parameter estimation. Weighted ridge regression was used because the competition kernel is high-dimensional and potentially collinear, with multiple singular vectors representing closely related competitive gradients [58]. Ridge regularisation stabilises coefficient estimates under such multicollinearity by penalising extreme solutions and shrinking coefficients towards zero. It also reduces the risk of overfitting associated with the relatively large number of predictors compared with the effective sample size available for trait estimation. The optimal combination of SVD rank and ridge penalty was selected by five-fold cross-validation across species, maximising the mean species-weighted coefficient of determination (R^2), averaged across functional traits and validation folds.

2.3. Competitive and Environmental Adversity Indication

Competitive and environmental adversity are hypothesised to contribute to the structuring of plant communities. The observed variation in community composition was characterised using multivariate ordination, while Grime's plant ecological strategies (CSR) were applied to interpret the resulting community gradients. Plant ecological strategies were characterised and quantified using species-level competitor (C), stress-tolerator (S), and ruderal (R) scores derived from the European dataset developed within the global CSR classification framework of Pierce et al. [59]. The competitor, stress-tolerator, and ruderal values of plant species [59], expressed as proportions that sum to 1, were subjected to a weighted mean procedure based on plant percentage cover. These estimates were subsequently normalised so that they sum to unity for each vegetation relevé. Since the sum of species percentage covers does not necessarily equal 100% due to visual estimation uncertainty and overlapping plant canopies, the resulting community-level CSR components were normalised to sum to unity, preserving their compositional nature before applying the isometric log-ratio (ilr) transformation. The isometric log-ratio (*ilr*) transformation was applied to obtain orthonormal coordinates [60]. The first *ilr* axis is derived by contrasting the proportion of competitors against the geometric mean of the proportions of stress-tolerators and ruderals, and was interpreted as an indicator of the competitive adversity gradient:

$$\text{Competive adversity} = \sqrt{\frac{2}{3}}\ \ln\left(\frac{C}{\sqrt{SR}}\right),$$

where C, S, and R represent the relative proportions of competitor, stress-tolerator, and ruderal strategies in the community, respectively (C + S + R = 1).

The second *ilr* axis contrasts stress-tolerators and ruderals, and was interpreted as an indicator of the environmental adversity gradient:

$$\text{Environmental adversity} = \sqrt{\frac{1}{2}}\ \ln\left(\frac{S}{R}\right).$$

2.4. Statistical Calculation

In the statistical models, the standardized effect sizes (SES) of functional diversity, calculated using different null models, were treated as response variables. Environmental adversity and competitive adversity were used as explanatory variables to assess their individual and interactive effects on functional trait convergence and divergence. The analyses were conducted separately for the different functional trait components and randomisation models.

To account for potentially complex and nonlinear relationships between trait dispersion and environmental or competitive adversity [32], Hierarchical General Additive Models (HGAM) were applied to capture potentially complex response forms [61]. Using a set of HGAM formulations enables testing the robustness of the patterns predicted by the stress–dominance hypothesis while accounting for site-specific conditions [17,61]. In practice, the HGAM framework was implemented by comparing six alternative model structures. These included a null model with no trend (null), a model with a single global smooth only (G), its time-augmented counterpart with an additional random-effect term for time (GT), a model combining a global smooth with site-specific deviations represented as a factor–smooth interaction (GS), and two time-augmented versions of the global-plus-site model that included the random-effect term for time, either with shared smoothness across sites (GST) or with site-specific smooths allowed to differ in shape (GIT). In addition, two models without a global smooth were considered, comprising a factor–smooth interaction for site (ST) and site-specific smooths (IT), both of which included the random-effect term

for time. The most parsimonious model among these candidates was selected using the corrected Akaike information criterion (AICc) [62]. The six HGAM formulations represent increasingly flexible ways of describing how trait convergence/divergence responds to gradients of environmental or competitive adversity while accounting for potential differences among sites. Comparison of these alternative structures allows an expanded set of questions concerning both spatial and temporal structure to be addressed: (1) Does any systematic trend exist at all? (2) Is there a common underlying trend shared across sites? (3) If sites differ, do these differences reflect shifts in magnitude only, or differences in the shape/complexity of the response curve? (4) Do observations taken at the same time share additional variability beyond the fitted smooth components, indicating a coherent time-structured signal across sites? The null model tests whether the data support any systematic pattern. The site-only models (IT and ST) evaluate whether each site follows its own response, either with flexible site-specific shapes (IT) or with comparable smoothness enforced across sites (ST). The global-trend models (G and GS) test whether a common pattern exists across sites, with GS allowing structured site-specific deviations around the global smooth. The time-augmented counterparts (GT, GST, and GIT) additionally include a random-effect term for time, enabling separation of the smooth component(s) from variability shared among observations within the same time step. Selecting the most parsimonious model using AICc therefore provides a principled way to assess the generalizability of the stress–dominance pattern while accounting for time-structured heterogeneity. The dataset and R code used for the HGAM analyses are publicly available in the Zenodo repository [63]. Pairwise beta diversity among sampling sites was quantified using the Arrhenius-based index implemented in the betadiver() function (method = "z") of the R package vegan version 2.7-2. Environmental and competitive adversity were analysed using Gaussian generalized linear mixed models fitted with the R package glmmTMB version 1.1.11. Environmental predictors and sampling time were considered as fixed effects, while alternative random-effect structures were evaluated to account for repeated observations and spatial dependence, including site-level random intercepts, first-order temporal autocorrelation [AR(1)], and spatial random fields with Matérn covariance. Candidate models were compared using the Akaike information criterion (AIC). Non-metric multidimensional scaling (NMDS) was performed on the species composition matrix using Bray–Curtis dissimilarities and a two-dimensional configuration (metaMDS, R package vegan) [64]. Environmental and competitive adversity were subsequently fitted onto the ordination as external variables using envfit, with significance assessed by 999 permutations. Pairwise PERMANOVA (adonis2) based on Bray–Curtis dissimilarity was used to evaluate differences in macrophyte species composition among waterbody types with statistical significance assessed using 999 permutations [65]. For each pair of types, the associated R^2 and permutation p-values were obtained [66]. Hierarchical generalized additive models (HGAMs) were fitted using the mgcv package version 1.9.1 in R. Thin-plate regression splines (bs = "tp") were used for global smooth functions, while factor-smooth interactions (bs = "fs") represented waterbody-type-specific responses. Where included, sampling month was modelled as a random intercept (bs = "re"). Candidate models differed in their inclusion of global smooths, waterbody-type-specific smooths, and temporal random effects. For the T2 response along the environmental adversity gradient, shape-constrained additive models (scam package version 1.2.20) were additionally fitted using a monotonic decreasing smooth. GAM smoothing parameters were estimated by restricted maximum likelihood (REML) [67].

2.5. Spatially Structured Variation

The spatially structured component of the variation in the standardised effect sizes (SES) was quantified by the application of Moran's eigenvector maps (MEM) [68,69]. The MEM variables represent orthogonal spatial predictors derived from the eigen-decomposition of a spatial weighting matrix and describe spatial structures at multiple scales, from broad to fine [70]. The spatial weighting matrix was computed using the Gabriel graph based on site coordinates, and was transformed into a matrix of centred spatial distances. The eigen-decomposition of this matrix produced a set of MEM eigen-functions (dbMEM variables), each associated with a specific spatial scale and a positive Moran's I value, ensuring that only positively autocorrelated spatial structures were retained for modelling [71]. The amount of SES variation explained by each MEM predictor was quantified using the redundancy analysis (RDA) models of the form:

$$\mathrm{SES} \sim \mathrm{MEM}_i,$$

and extracted the adjusted coefficient of determination (R^2_{adj}) for each MEM. The significance of each spatial predictor was evaluated using permutation tests (n = 999). MEM predictors were then grouped into three spatial scale classes according to their order in the eigen-spectrum: broad-scale (MEM 1–10), medium-scale (MEM 11–30), and fine-scale (MEM 31–485), reflecting long-wave, meso-scale, and short-wave spatial structures, respectively. This classification was heuristic, with boundaries selected based on the ordering of spatial eigenfunctions and visual inspection of their grouping to obtain interpretable spatial scale classes. The boundaries should therefore be regarded as approximate rather than representing objectively defined transitions between spatial scales. The pure spatial component controlling for environmental or competitive adversity was estimated by fitting the partial RDA models of the form:

$$\mathrm{SES} \sim \mathrm{MEM}_i + \mathrm{Condition}(\mathrm{Adversity}),$$

where the conditional variable represented either environmental adversity (for SES(T2)) or competitive adversity (for SES(Range) and SES(T4)). The adjusted partial R^2 values were used to quantify the spatial variation in SES that remained after accounting for variation shared with environmental or competitive gradients. For each spatial-scale class, statistically significant MEM variables were jointly included in a separate RDA model, and the adjusted R^2 of the resulting model was used to quantify the broad-, medium-, or fine-scale spatial variation in SES. These totals were expressed both as absolute explained variation and as proportions of the overall spatial variation. The calculations were performed in R [72] using the packages *vegan* version 2.7.2 for (partial) RDA and permutation tests [73], *adespatial* version 0.3.28 for computing Moran's eigenvector maps (dbMEM) [74], *spdep* version 1.4.1 for spatial weighting matrices and neighbourhood graphs (including the Gabriel graph) [75], and *ade4* version 1.7.23 for handling orthobasis objects [76].

2.6. Study Area and Sampling Design

The study was conducted in 2024 over four rounds of surveys: 6–10 May, 3–7 June, 15–19 July, 19–23 August, within the bodies of water of the Dnipro-Orilskiy Nature Reserve (Dnipropetrovska Oblast, Ukraine). The Dnipro-Orilskiy Nature Reserve was established in 1990 and encompasses an area of 3766 hectares. The reserve's bodies of water are located within the Dnipro Reservoir, part of the Dnipro River cascade of reservoirs. The total area of bodies of water within the reserve is 602.8 hectares. These bodies of water can be categorised into the following systems: the Dnipro riverbed (total area of 223.4 hectares), the Obukhivka ledge system (73.3 hectares), the Orilsky Canal (21.7 hectares), the Taromske ledge system (183.4 hectares), and the Mykolaivka ledge system (101.0 hectares) [77]. During each

survey round, aquatic macrophytes were recorded, and water properties were measured at 453 sampling locations.

2.7. Waterbody Morphology

The water bodies were classified into seven functional types: channels, bays, confluent lakes, contrafluent lakes, contrafluent–confluent lakes, isolated floodplain lakes, and artificial water bodies. The classification of floodplain lakes was based primarily on their hydrological connectivity and the predominant direction of water flow [78]. These categories represent differences in water exchange with the river system and associated hydrological conditions. Channels and bays constitute elements of the connected river–floodplain network, whereas isolated floodplain lakes lack direct surface-water connections with the river. Confluent, contrafluent, and contrafluent–confluent lakes represent distinct configurations of water exchange and flow direction. The waterbody types also differ in surface area, depth, volume, and shoreline morphology. Their detailed morphological and functional characteristics, as well as the procedures used to assess waterbody morphology and construct the digital elevation model, have been described in our previous studies [79–81]. The digital terrain model was integrated with the digital model of the reservoir bottom to produce a comprehensive digital elevation model that encompasses both above and below the water surface. A total of 312 bodies of water were identified within the study area. Among these, 93 (29.8%) were classified as Channels, 54 (17.3%) as Contrafluent lakes, 52 (16.7%) as Isolated floodplain lakes, 50 (16.0%) as Bays, 38 (12.2%) as Contrafluent-confluent lakes, 17 (5.5%) as Confluent lakes, and 8 (2.6%) as Artificial bodies of water (Figure 1). The morphometric characteristics of the bodies of water were calculated using the *lakemorpho* package version 1.3.2 [82]. These characteristics were then subjected to principal component analysis, resulting in the extraction of principal components with eigenvalues greater than 1 [81].

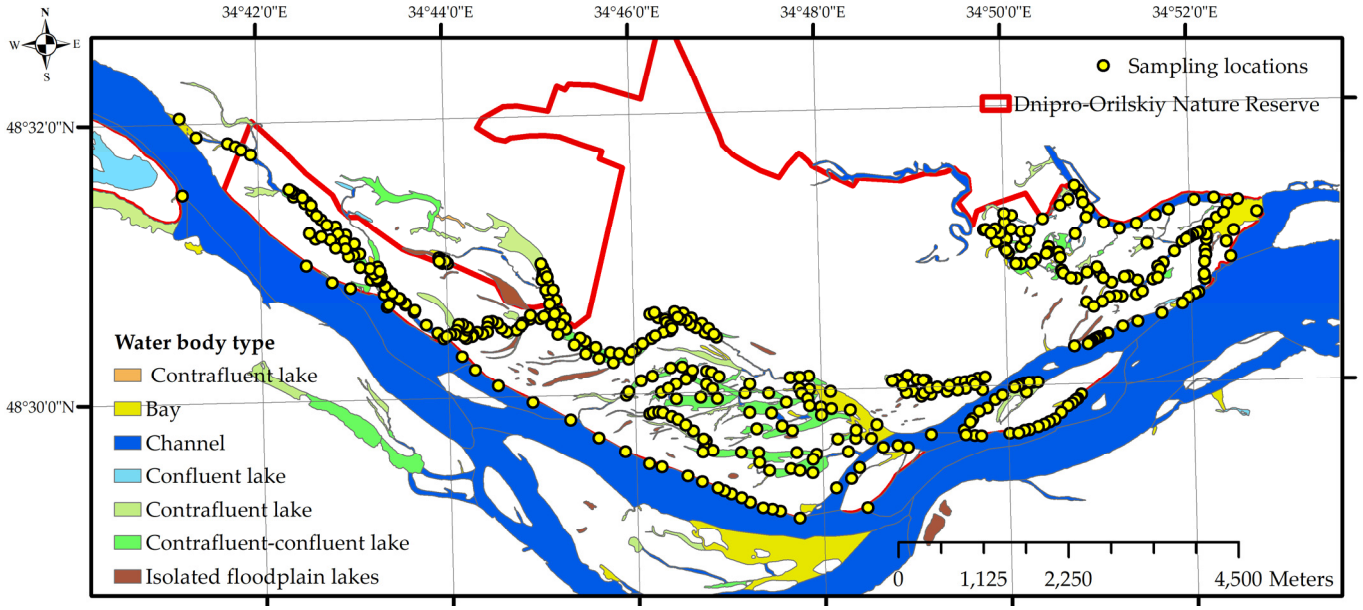


Figure 1. Map of the study area within the Dnipro-Orilskyi Nature Reserve, showing the spatial distribution of different waterbody types and the locations of macrophyte sampling sites. Waterbody types are distinguished by colour, yellow circles indicate sampling locations, and the red outline marks the boundary of the nature reserve.

2.8. Environmental Measurements

The electrical conductivity, temperature, water transparency, and dissolved oxygen content were measured at each monitoring location. The measurements were taken between 11 a.m. and 1 p.m., when the daily temperature variation was at its lowest. This time frame was selected because it provides the closest approximation to the maximum daily temperatures. The electrical conductivity of the water was measured using a portable conductivity meter (HI 993310, Hanna Instruments, Woonsocket, RI, USA). The dissolved oxygen content was assessed with a Hanna HI 98193 oximeter (Hanna Instruments, Woonsocket, RI, USA). Water temperature and pH were measured using a Hanna 98107 pH meter (Hanna Instruments, Woonsocket, RI, USA). Water transparency was evaluated using a Secchi disc (Hach Company, Loveland, CO, USA) [83].

2.9. Plants' Functional Traits

A total of 100 plant species were identified due to the surveys. The following traits are considered as functional characteristics of plants: flower sexual syndrome [84], Raunkiær plant life-form [85], pollenochores, diasporochores (ecobiochores) [86,87], plant height, leaf area, specific leaf area, leaf thickness [84], leaf type [88], leaf water content per leaf dry mass [84], leaf nitrogen content per leaf dry mass, seed dry mass, seed number per plant, leaf carbon/nitrogen (C/N) ratio, flowering time, fruit size [84], body flexibility [88], vertical shoot architecture [88], rooting at nodes, below-ground to above-ground biomass ratio, life span [84], dispersal distance class [89], growth form [88], mode of reproduction [88], number of reproductive organs [88], leaf texture [88], leaf cover [88]. Community-level ecological indicator values were calculated using the Ellenberg-type indicator values for European vascular plant species [90]. For each ecological factor, community-weighted mean indicator values were calculated using species percentage cover as weights. he complete species-by-traits matrix, together with trait definitions, measurement units, and explanations of categorical variables, is publicly available in the Zenodo repository [91].

3. Results

3.1. Species Richness and Community Composition Across Waterbody Types

A total of 100 aquatic macrophyte species were recorded across the reserve's water bodies. Species richness varied among waterbody types: 86 species were found in contrafluent–confluent lakes, 88 in channels, 68 in contrafluent lakes, 65 in bays, 49 in confluent lakes, and 38 species each in isolated floodplain lakes and artificial quarries. The Arrhenius-based β-diversity values showed considerable variation across site pairs, ranging from 0.00 to 0.96, with a median of 0.51 (25th and 75th percentiles: 0.43 and 0.60, respectively). Pairwise PERMANOVA indicated weak to moderate but statistically significant differences in macrophyte species composition among waterbody types (R^2 = 0.01–0.43; all $p < 0.05$) (Table 1).

Table 1. Pairwise PERMANOVA results for macrophyte species composition among waterbody types. The upper-right triangle presents R^2 values, with asterisks indicating statistical significance (*** $p = 0.001$). Diagonal and lower-left entries are shown as "—".

Waterbody Type	Artificial Quarry	Bay	Channel	Confluent Lake	Contrafluent–Confluent Lake	Contrafluent Lake	Isolated Floodplain Lakes
Artificial quarry	—	0.092 ***	0.023 ***	0.270 ***	0.022 ***	0.073 ***	0.432 ***
Bay	—	—	0.038 ***	0.067 ***	0.015 ***	0.068 ***	0.154 ***
Channel	—	—	—	0.025 ***	0.039 ***	0.042 ***	0.032 ***
Confluent lake	—	—	—	—	0.011 ***	0.027 ***	0.250 ***

Table 1. *Cont.*

Waterbody Type	Artificial Quarry	Bay	Channel	Confluent Lake	Contrafluent–Confluent Lake	Contrafluent Lake	Isolated Floodplain Lakes
Contrafluent–confluent lake	—	—	—	—	—	0.017 ***	0.028 ***
Contrafluent lake	—	—	—	—	—	—	0.065 ***
Isolated floodplain lakes	—	—	—	—	—	—	—

3.2. Spatiotemporal Patterns of Environmental and Competitive Adversity

Gaussian GLMMs indicated that both environmental and competitive adversity, expressed in terms of isometric log-ratio coordinates, exhibited significant temporal autocorrelation and a non-negligible spatial random field (Table 2). Environmental adversity increases with higher pH, Ellenberg indicator values for light, continentality, acidity and salinity, and decreases with Ellenberg humidity. In contrast, sampling month and water body type do not show significant fixed effects on environmental adversity. The environmental adversity is clearly heterogeneous along the floodplain, forming coherent patches that persist across months rather than a uniform gradient (Figure 2).

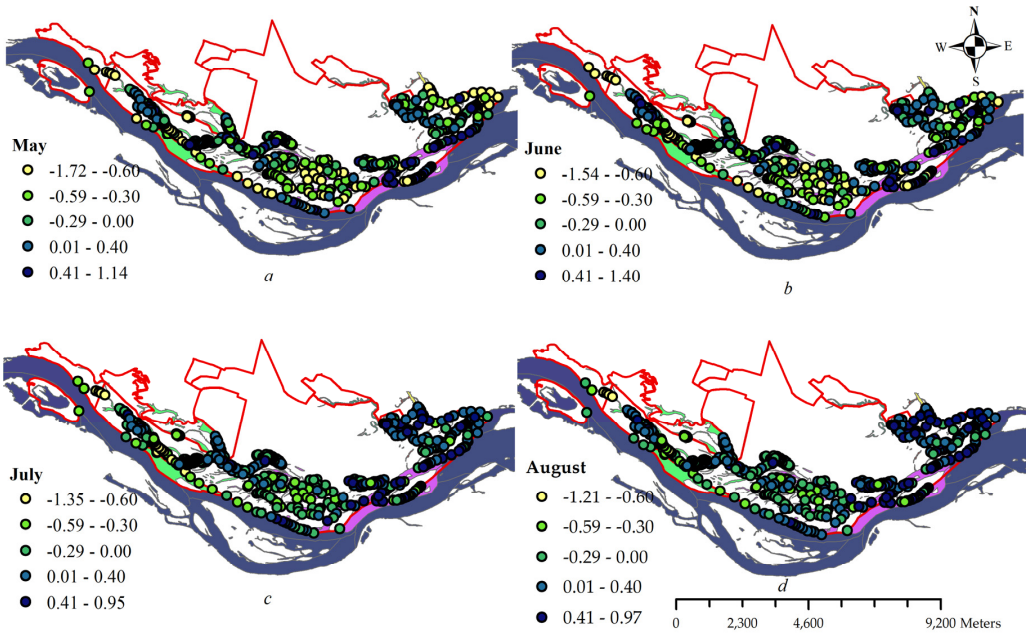


Figure 2. Spatial variation in environmental adversity across four sampling periods: (**a**) May, (**b**) June, (**c**) July, and (**d**) August. Points indicate sampling locations where aquatic macrophyte communities were surveyed and environmental properties were measured. Environmental adversity is expressed as a dimensionless isometric log-ratio coordinate derived from community-level CSR strategy composition; higher values indicate greater environmental adversity. The dark blue background represents the river channel, while the red line indicates the boundaries of the Dnipro–Oril Nature Reserve. The same 453 sampling locations were surveyed during each sampling period. Floodplain water bodies are shown in green.

Competitive adversity increases with higher water temperature and with higher Ellenberg indicator values for light, temperature, and humidity, and decreases with higher Ellenberg values for continentality, acidity, and salinity (Table S1). Water body type does not show significant fixed effects on competitive adversity. Over the study period, competitive adversity tended to increase, as reflected in the statistically significant positive effect of August relative to May. Competitive adversity shows marked patchiness across

the floodplain, with clusters of higher and lower values that remain recognisable between months despite the overall seasonal increase (Figure 3).

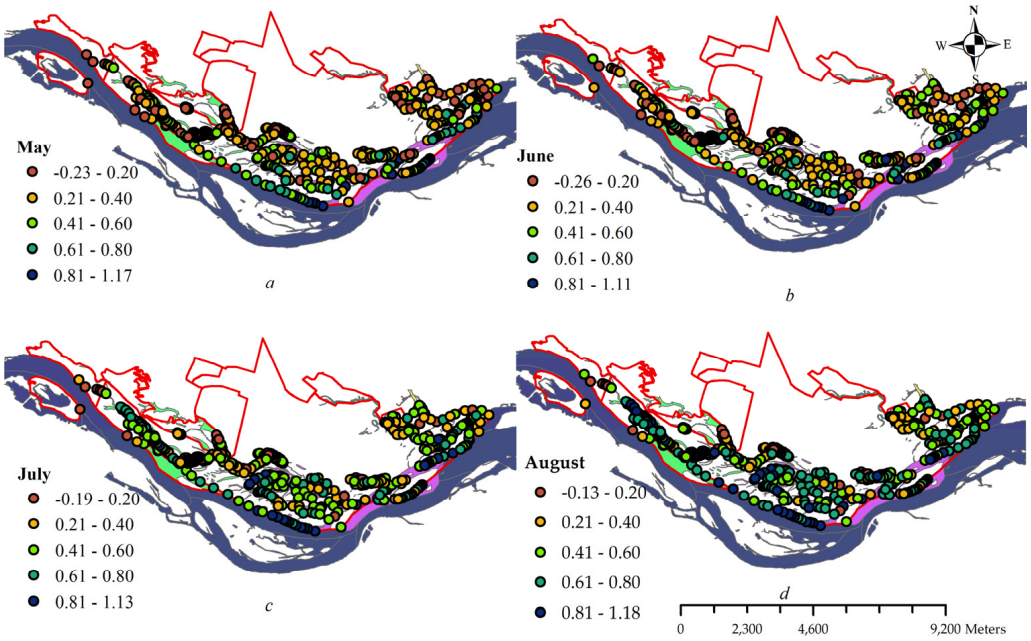


Figure 3. Spatial variation in competitive adversity across four sampling periods: (**a**) May, (**b**) June, (**c**) July, and (**d**) August. Points indicate sampling locations where aquatic macrophyte communities were surveyed and environmental properties were measured. Competitive adversity is expressed as a dimensionless isometric log-ratio coordinate derived from the composition of community-level CSR strategies; higher values indicate greater competitive adversity. The dark blue background represents the river channel, while the red line indicates the boundaries of the Dnipro–Oril Nature Reserve. The same 453 sampling locations were surveyed during each sampling period. Floodplain water bodies are shown in green.

Table 2. Fixed effects of the Gaussian GLMM for environmental and competitive adversities (N = 1812 observations in 453 sites).

Term		Environmental Adversity Temporal Autocorrelation (ρ = 0.57, 95% CI [0.48; 0.64]) and a Spatial Random Field (σ_{sp} = 0.276) logLik = 723.8; AIC = −1391.7; BIC = −1237.6					Competitive Adversity Temporal Autocorrelation (ρ = 0.53, 95% CI [0.45; 0.60]) and a Spatial Random Field (σ_{sp} = 0.118) logLik = 1946.0; AIC = −3835.9; BIC = −3681.9				
		Est ± SE	z Value	*p*–Value	CI Lower	CI Upper	Est ± SE	z Value	*p*–Value	CI Lower	CI Upper
Intercept		−0.115 ± 0.143	−0.808	0.419	−0.395	0.164	0.411 ± 0.061	6.712	<0.001	0.291	0.532
Environment parameters	Temp	0.014 ± 0.013	1.037	0.300	−0.012	0.040	0.017 ± 0.007	2.413	0.016	0.003	0.031
	Transp	−0.014 ± 0.007	−1.897	0.058	−0.028	0.000	−0.003 ± 0.004	−0.761	0.447	−0.010	0.005
	EC	0.008 ± 0.018	0.473	0.636	−0.026	0.043	0.011 ± 0.009	1.18	0.238	−0.007	0.029
	Ox	0.005 ± 0.006	0.834	0.404	−0.007	0.018	0.003 ± 0.003	0.94	0.347	−0.003	0.010
	pH	0.021 ± 0.008	2.631	0.009	0.005	0.037	0.007 ± 0.004	1.685	0.092	−0.001	0.015
Ellenberg indicator values	Light regime	0.140 ± 0.008	16.836	<0.001	0.123	0.156	0.102 ± 0.004	24.359	<0.001	0.094	0.11
	Temperatures	0.013 ± 0.008	1.554	0.12	−0.003	0.030	0.037 ± 0.004	8.582	<0.001	0.028	0.045
	Continentality	0.087 ± 0.008	10.525	<0.001	0.07	0.103	−0.038 ± 0.004	−8.971	<0.001	−0.046	−0.029
	Humidity	−0.122 ± 0.010	−12.711	<0.001	−0.141	−0.104	0.087 ± 0.005	17.683	<0.001	0.077	0.097
	Acidity	0.043 ± 0.010	4.488	<0.001	0.024	0.061	−0.055 ± 0.005	−11.313	<0.001	−0.065	−0.045
	Nutrients	0.006 ± 0.009	0.597	0.55	−0.013	0.024	−0.001 ± 0.005	−0.191	0.848	−0.010	0.008
	Salinity	0.219 ± 0.008	26.655	<0.001	0.203	0.235	−0.058 ± 0.004	−13.763	<0.001	−0.066	−0.049
Time (month; May is the reference)	June	0.014 ± 0.047	0.299	0.765	−0.078	0.106	0.012 ± 0.025	0.494	0.621	−0.036	0.061
	July	0.010 ± 0.065	0.152	0.879	−0.117	0.136	0.034 ± 0.034	0.998	0.318	−0.032	0.1
	August	0.065 ± 0.063	1.041	0.298	−0.058	0.189	0.073 ± 0.033	2.237	0.025	0.009	0.138

Table 2. *Cont.*

Term		Environmental Adversity Temporal Autocorrelation (ρ = 0.57, 95% CI [0.48; 0.64]) and a Spatial Random Field (σ_{sp} = 0.276) logLik = 723.8; AIC = −1391.7; BIC = −1237.6					Competitive Adversity Temporal Autocorrelation (ρ = 0.53, 95% CI [0.45; 0.60]) and a Spatial Random Field (σ_{sp} = 0.118) logLik = 1946.0; AIC = −3835.9; BIC = −3681.9				
		Est ± SE	z Value	*p*–Value	CI Lower	CI Upper	Est ± SE	z Value	*p*–Value	CI Lower	CI Upper
Water body types (Artificial water bodies are referencing)	Bay	−0.106 ± 0.106	−1.001	0.317	−0.315	0.102	0.005 ± 0.049	0.112	0.911	−0.091	0.102
	Channel	−0.042 ± 0.094	−0.447	0.655	−0.227	0.143	0.022 ± 0.044	0.507	0.612	−0.064	0.108
	Confluent lake	−0.171 ± 0.120	−1.422	0.155	−0.406	0.065	−0.045 ± 0.056	−0.803	0.422	−0.154	0.065
	Contrafluent-confluent lake	−0.027 ± 0.099	−0.272	0.786	−0.222	0.168	0.037 ± 0.046	0.795	0.426	−0.054	0.127
	Contrafluent lake	0.003 ± 0.104	0.027	0.978	−0.201	0.207	0.000 ± 0.048	0.005	0.996	−0.094	0.095
	Isolated floodplain lakes	−0.140 ± 0.163	−0.859	0.39	−0.46	0.180	−0.115 ± 0.077	−1.490	0.136	−0.266	0.036

The NMDS ordination reveals that the first axis (NMDS1) is positively correlated with competitive adversity, whereas the second axis (NMDS2) aligns with the gradient of environmental adversity (Figure 4). The total weighted inertia of the species-by-traits matrix was SS_{tot} = 74.7. Of this amount, the environment-sensitive component extracted by the RLQ projection accounted for SS_{env} = 16.3, i.e., 21.8% of the total trait inertia. The competition-related component of the traits matrix reconstructed from the interaction kernel contributed only 9.4, corresponding to 12.6% of the total inertia. The remaining SS_{resid} = 49.1 (65.7%) of the trait variation was unexplained by either the environment or the fitted competition model.

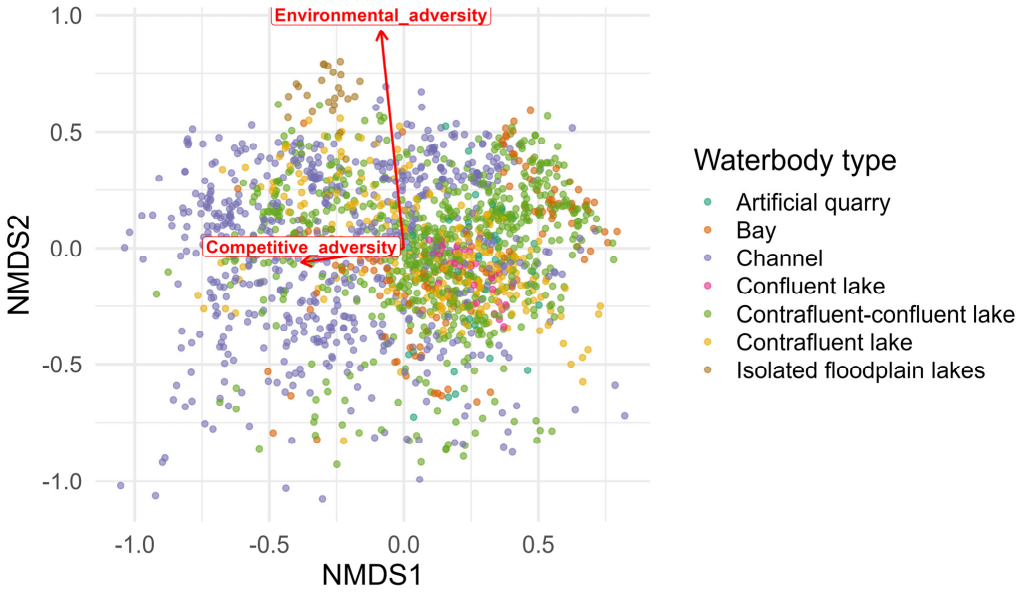


Figure 4. Non-metric multidimensional scaling (NMDS, Bray–Curtis distance, k = 2; stress = 0.228) of aquatic macrophyte species composition in different waterbody types. Points are coloured by waterbody type; red arrows indicate fitted gradients of competitive and environmental adversity (envfit, r^2 = 0.076, p = 0.001 for competitive adversity; r^2 = 0.448, p = 0.001 for environmental adversity).

3.3. Environmental and Competition-Related Components of Functional Trait Variation

Functional traits exhibited varying degrees of sensitivity to environmental conditions and competitive interactions, as reflected in the relative contributions of these components to trait variation (Table S2). The highest proportions of trait variation explained by the environmental component were observed for geophyte life-forms (0.65; values in parentheses here

and below indicate proportions of explained trait variation), barochorous dispersal (0.62), nitrogen content (0.59), traits associated with a single basal growth point (0.54), perennial life span (0.47), tubular leaves (0.30), capillary leaves (0.22–0.30), and several reproductive traits, such as very high numbers of reproductive organs (0.65) and large tubers (0.65). The traits most sensitive to interspecific competition included epizoochorous dispersal (0.25), endozoochory (0.27), therophyte life-forms (0.16), leaf water content per dry mass (0.31), nodes (0.15), annual life span (0.31), and competitive pollination or dispersal modes such as gametohydrophily (0.17). Several traits, such as nanophanerophytic life-forms, hydrophilous pollination, anemochorous dispersal, biennial life span, free-floating submerged growth forms, and reproductive modes such as rhizomes or budding, were characterised by a high proportion of unexplained (residual) variance, indicating that their variation is only weakly aligned with the environmental gradients and competition kernel considered here.

3.4. Statistical Power of Randomisation Models and Selection of Adversity–Response Models

Power analysis and simulated effect sizes for the alternative community assembly scenarios (Table S3) identified the randomisation models most sensitive to detecting the different assembly mechanisms. The T2 randomisation model, which utilises environment-sensitive traits, demonstrated the greatest power in detecting environmental filtering. The Range randomisation model, which employs competition-sensitive traits, was most effective in the scenario where the competition trait is divergent under symmetric competition. The T4 randomisation model, based on residual traits, performed best in the scenario where the competition trait is convergent under asymmetric competition.

Model selection based on the corrected Akaike Information Criterion (AICc) across hierarchical GAM formulations describing the responses of three effect sizes to competitive and environmental adversity gradients revealed clear differences among response variables and gradients. For Range along the competitive adversity gradient, the lowest AICc was obtained by the GST model, indicating that the data are best explained by a shared global nonlinear trend complemented by type-specific deviations and an additional random effect of sampling time (Table 3).

Table 3. Corrected Akaike information criterion (AICc) values for hierarchical GAM models relating trait convergence/divergence (Range, T4 and T2) to competitive and environmental adversity gradients. Bold values indicate the most parsimonious model (i.e., the model with the lowest AICc); numbers in parentheses give ΔAICc relative to the best model.

Model	Range (Competitive Adversity)	T2 (Environmental Adversity)	T4 (Competitive Adversity)	T4 (Environmental Adversity)
Null	5333.230 (495.981)	10,709.968 (263.206)	10,195.434 (308.165)	10,195.434 (224.172)
G	5093.204 (255.955)	10,612.793 (166.031)	10,024.915 (137.645)	10,139.616 (168.354)
GT	5094.530 (257.281)	10,611.825 (165.062)	10,019.898 (132.628)	10,135.444 (164.183)
GS	4847.134 (9.886)	10,448.469 (1.706)	9889.604 (2.334)	9975.968 (4.706)
GST	**4837.248**	**10,446.763**	**9887.270**	9971.912 (0.650)
GIT	4929.514 (92.266)	10,545.413 (98.651)	9983.125 (95.856)	10,075.594 (104.332)
ST	4837.608 (0.359)	10,453.024 (6.261)	9894.597 (7.328)	**9971.262**
IT	4902.838 (65.589)	10,530.019 (83.256)	9992.766 (105.496)	10,063.620 (92.358)

For T4 along the competitive adversity gradient, the GST model was again favoured, supporting the same interpretation of a common overall trend with systematic differences among waterbody types and a temporal random component. For T2 along the environmental adversity gradient, the GST model had the lowest AICc. In contrast, the GS model was within 2 AICc units, suggesting that adding the temporal random effect yields only a marginal improvement over the purely spatially structured global-plus-type formulation. Therefore,

the dominant signal in T2 appears to be spatial rather than temporal. In contrast, for T4 along the environmental adversity gradient, the most parsimonious model was ST, which excludes a global smooth and represents the relationship entirely via type-specific smooth responses, together with the random effect of time. This indicates that the T4 response to environmental adversity is primarily type-dependent, with no single transferable global trend across waterbody types. Consistent with the small AICc gain from including time for T2, the fitted response curves were very similar among months (Figure S1), implying that temporal variation is weak and not readily distinguishable by visual inspection. Accordingly, GS-type formulations were emphasised for spatial-profile visualisations, while AICc-best models were retained for inference where they differed from the corresponding GS models.

3.5. Trait Convergence and Divergence Along Environmental and Competitive Adversity Gradients

GAM predictions obtained without including site and time as predictors revealed distinct patterns of trait convergence and divergence along environmental and competitive adversity gradients (Figure 5).

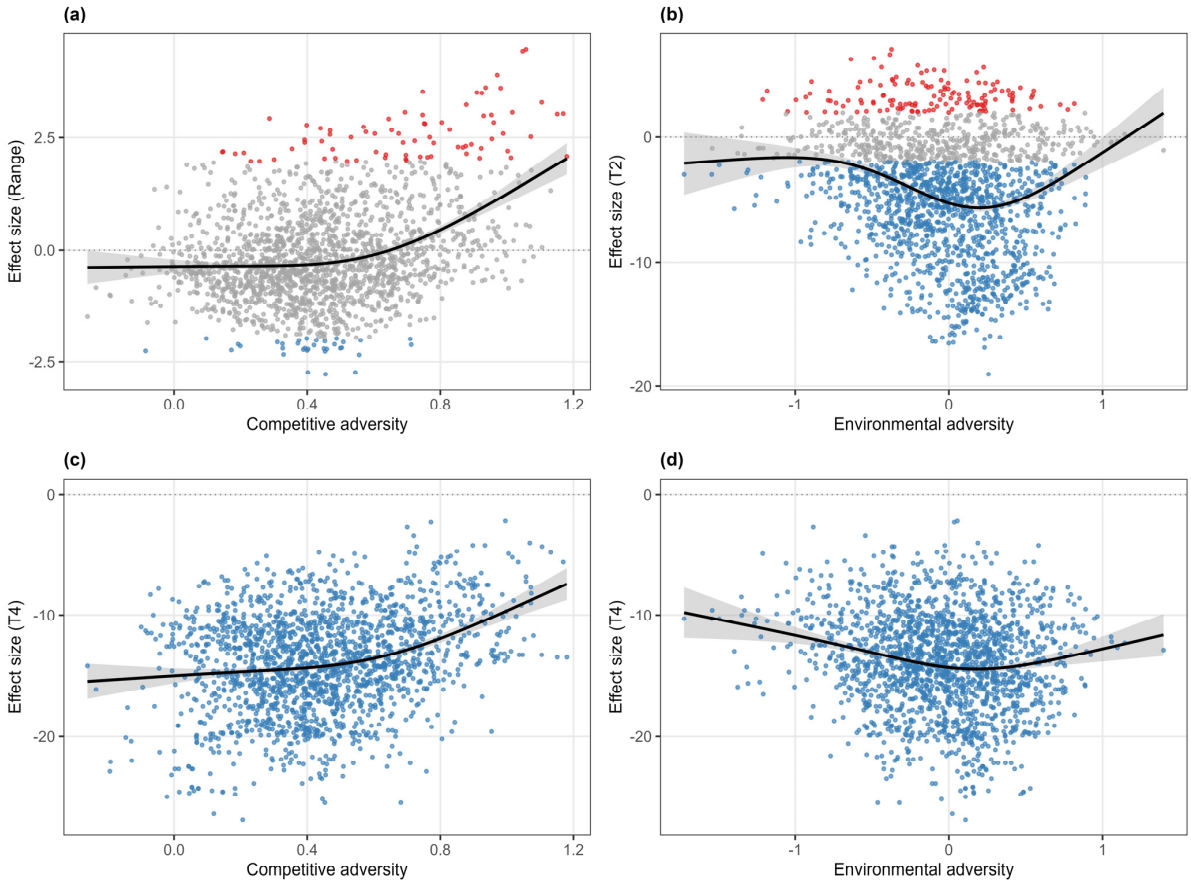


Figure 5. Global relationships between plot-level trait convergence/divergence effect sizes and adversity gradients derived from the global GAM models (G). Blue points indicate trait convergence (SES < -1.96), red points indicate trait divergence (SES > 1.96), and grey points indicate effect sizes within the interval $-1.96 \leq$ SES ≤ 1.96. Black lines represent fitted global smooths, and grey ribbons indicate 95% confidence intervals of the predictions. (**a**) Range effect sizes along the competitive adversity gradient; (**b**) T2 effect sizes along the environmental adversity gradient; (**c**) T4 effect sizes along the competitive adversity gradient; (**d**) T4 effect sizes along the environmental adversity gradient.

The effect sizes derived from the Range randomisation model, which employs competition-sensitive traits, exhibited an apparently random pattern at low levels to intermediate levels of competitive adversity but increased sharply with increasing adversity,

indicating trait divergence driven by limiting similarity (Figure 5a). The effect sizes derived from the T2 randomisation model, which utilises environment-sensitive traits, showed a seemingly random pattern at low levels of environmental adversity. However, at high levels of environmental adversity, effect sizes decreased sharply, indicating trait convergence driven by environment filtering (Figure 5b). The effect sizes derived from the T4 randomisation model, based on residual traits, were predominantly negative and exhibited a structured relationship with competitive adversity (Figure 5c). With increasing competitive adversity, effect sizes became less negative (i.e., their absolute magnitude decreased), but the relationship remained clearly structured rather than random. The relationship between T4 effect size and environmental adversity was nonlinear and non-monotonic (Figure 5d). The fitted curve exhibited a shallow mid-gradient minimum, while substantial variation in effect sizes was observed across the gradient. This indicates that a global environmental-adversity trend is not the dominant factor structuring T4. In contrast, the more consistently structured pattern is associated with competitive adversity (cf. Figure 5c). Models incorporating waterbody-type-specific smooths consistently outperformed the global smooth models according to AICc (Table S4). The GS model provided the best fit for Range (AICc = 4846.94, adjusted $R^2 = 0.246$) and T4 (AICc = 9891.08, adjusted $R^2 = 0.162$), whereas the S model was marginally preferred for T2 (AICc = 10454.08, adjusted $R^2 = 0.141$). The difference between the S and GS models for T2 was negligible (ΔAICc = 0.53). In the GS models, the global smooth was approximately linear for Range (edf = 1.00, F = 17.78, $p < 0.001$) and T2 (edf = 1.00, F = 6.46, $p = 0.011$), but nonlinear for T4 (edf = 2.74, F = 13.71, $p < 0.001$). Waterbody-type-specific smooth components were statistically significant in all three models ($p < 0.001$), with aggregate edf values of 21.76, 9.05, and 16.62 for Range, T4, and T2, respectively. The moderate explanatory power of the models (adjusted $R^2 = 0.141$–0.246 for the best-supported models) indicates substantial residual variation, although the fitted relationships were statistically supported.

3.6. Waterbody-Type-Specific Patterns of Trait Convergence and Divergence

Model-based analyses indicate that trait responses are shaped by both an overarching adversity-gradient signal and waterbody-type-specific deviations from this general trend. Two principal response patterns were evident across waterbody types (Figure 6). In some habitats, effect sizes declined almost steadily along the environmental adversity gradient (e.g., confluent lakes, contrafluent lakes, isolated floodplain lakes), suggesting that communities converged more strongly as conditions became harsher. Other habitats, however, exhibited weakly sigmoidal or clearly non-monotonic curves (e.g., artificial quarries, bays, channels, contrafluent–confluent lakes), with T2 remaining nearly unchanged at low adversity before flattening or even reversing at the upper end of the gradient. Taken together, these patterns demonstrate that both the strength and the form of trait responses to environmental adversity vary among waterbody types, although several waterbody types exhibit a progressive increase in trait convergence with increasing environmental adversity.

The communities exhibited three distinct behavioural patterns along the competitive adversity gradient for the Range randomisation model (Figure 7). In certain habitats, notably channel-like systems, effect sizes appeared almost indifferent to competition, displaying nearly flat relationships across the entire gradient. Other waterbody types remained unresponsive at low to intermediate adversity but 'activated' under stronger competitive conditions, with effect sizes increasing only at high values (e.g., bay, contrafluent–confluent lakes). By contrast, confluent lakes and isolated floodplain lakes showed an approximately monotonic increase in Range effect sizes across the full gradient, signalling progressively stronger divergence towards higher competitive adversity.

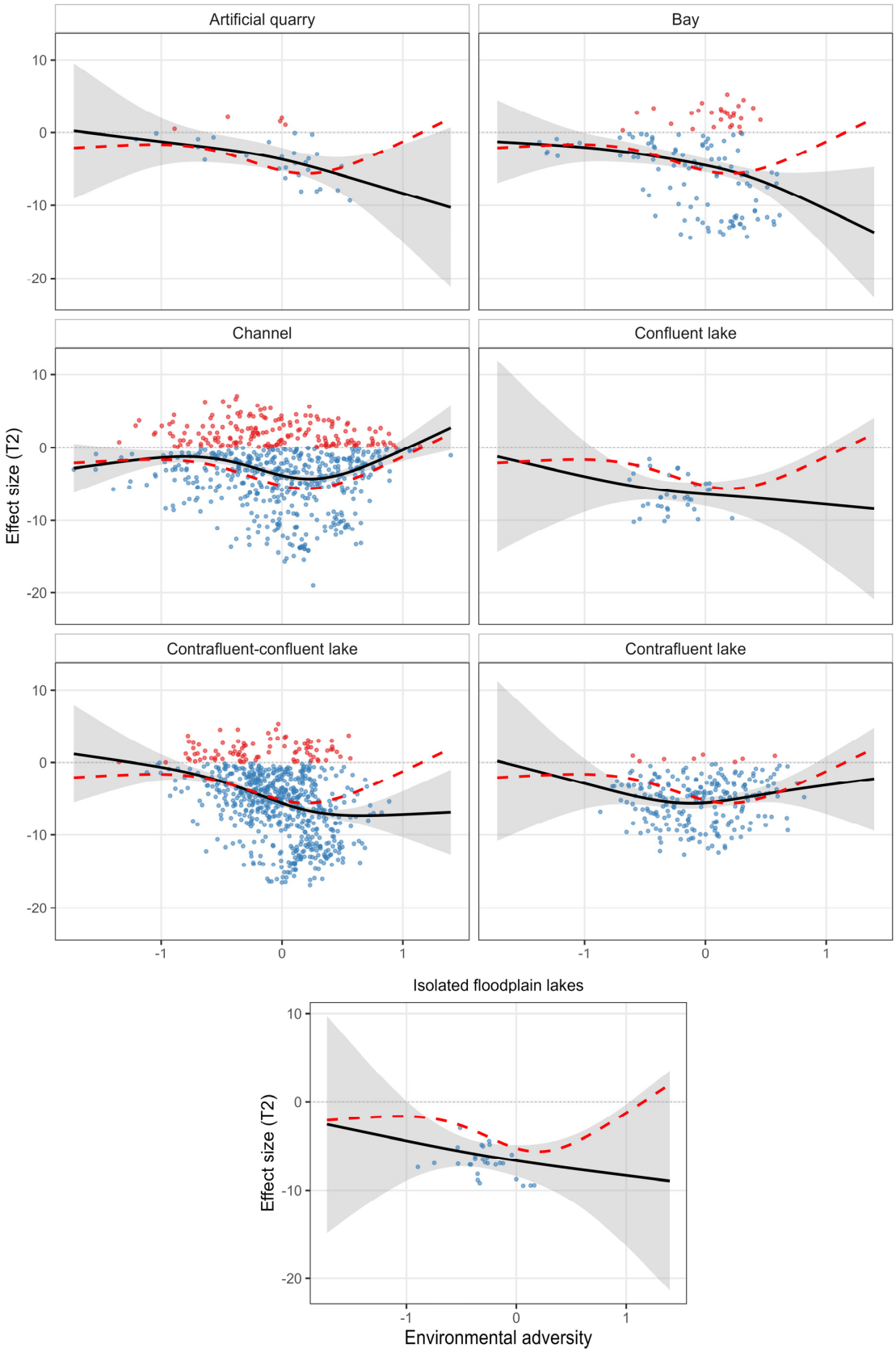


Figure 6. Global relationships between plot-level trait convergence/divergence effect sizes and adversity gradients derived from the global GAM models (G). Red points indicate statistically significant trait divergence (SES > 1.96), whereas light blue points represent all other effect sizes (SES ≤ 1.96), including statistically significant trait convergence (SES < −1.96). Black lines represent fitted smooths, and grey ribbons indicate 95% confidence intervals of the predictions.

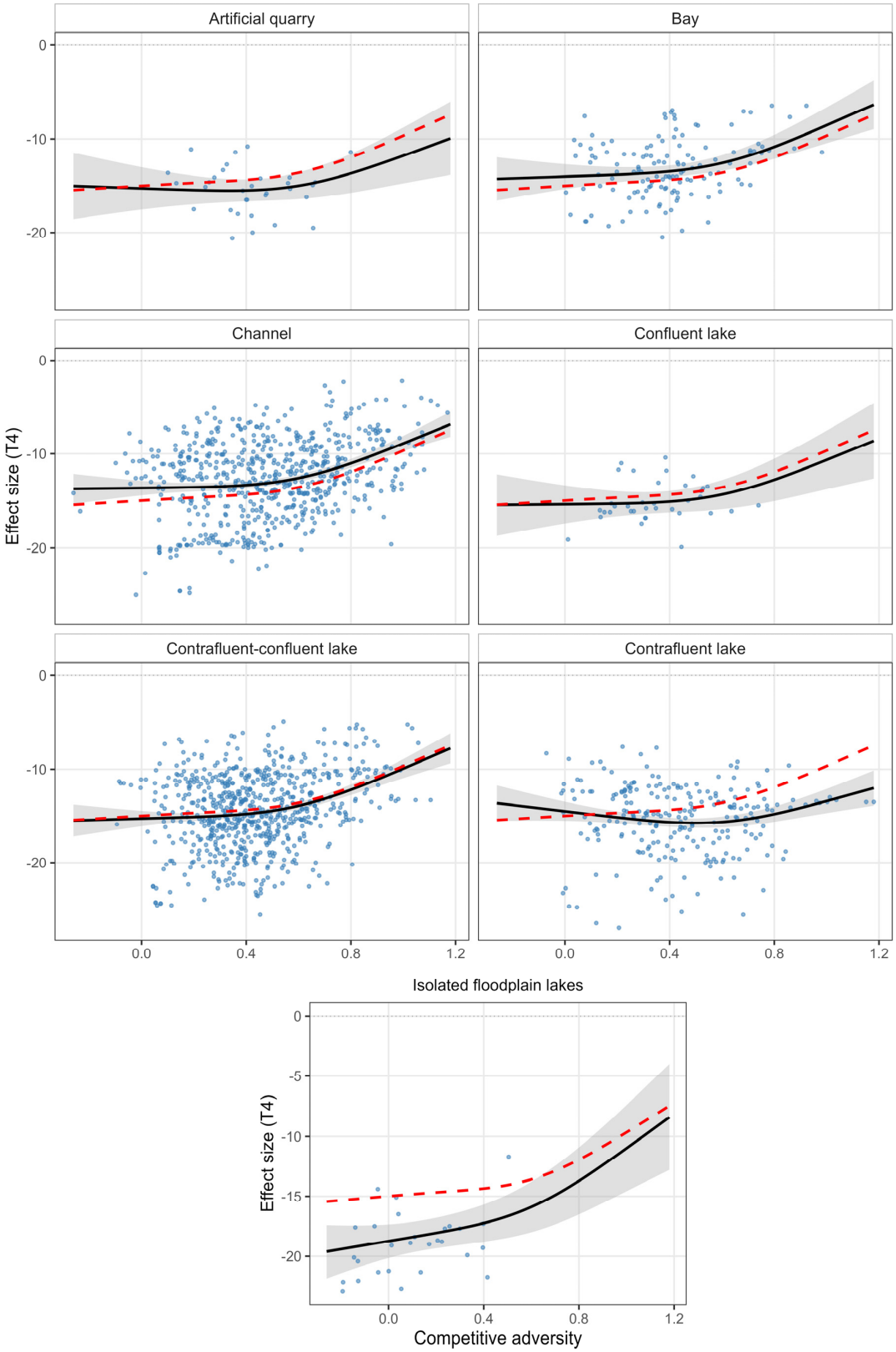


Figure 7. Global relationships between plot-level trait convergence/divergence effect sizes (Range) and competitive adversity across different waterbody types. Light blue points represent observed plot-level effect sizes (SES). Black lines represent fitted curves from the GS model (global smooth with waterbody-type-specific deviations), grey ribbons indicate 95% confidence intervals, and red dashed lines represent predictions from the global G model.

T4 effect sizes revealed a closely related, though not identical, pattern. Channel-like waterbodies exhibited little response to the competitive gradient, with flat or only slightly varying curves (e.g., channels). Several habitats exhibited muted responses at low and intermediate levels of adversity, followed by a steep, late increase at the upper end (e.g., bays, contrafluent–confluent lakes). In others, including confluent lakes and isolated floodplain lakes, T4 increased more smoothly and almost monotonically along the gradient, indicating that divergence strengthened steadily as competitive adversity intensified.

3.7. Spatial Structure of Trait Convergence and Divergence

The MEM-based spatial modelling revealed that a substantial proportion of the SES variation was spatially structured (Figure 8). Depending on the SES metric, the total amount of spatial variation explained by the MEM predictors ranged from 0.49 (Range) to 0.68 (T2) and 0.63 (T4), indicating that spatial processes represent a major component of the observed ecological patterns (Table 4). The scalograms, which illustrate the individual contributions of each MEM variable to the SES variation, were examined to interpret better the distribution of spatial variation across different spatial scales (Figure 8). The spatial structures were classified into three scale categories based on the characteristic ordering of MEM eigenfunctions: broad-scale (MEM 1–10), medium-scale (MEM 11–30), and fine-scale (MEM 31–485). These scale categories correspond to broad-, medium-, and fine-scale spatial patterns, respectively, and capture distinct ecological processes operating at different spatial domains.

Table 4. Spatial variation in standardised effect sizes (SES) explained by MEM-based spatial predictors before and after accounting for environmental or competitive adversity. Broad-, medium-, and fine-scale components correspond to MEM variables 1–10, 11–30, and 31–485, respectively. Total adjusted R^2 was estimated using all MEM predictors simultaneously. The contributions of individual spatial scale classes were calculated using Shapley decomposition, which distributes shared explained variation among scale classes. Pure spatial variation represents the unique spatial contribution after accounting for the corresponding adversity gradient. Percentage values indicate the relative contributions of each spatial scale class to the total spatial variation.

Randomisation Model (SES)	Scale Class	R^2_{adj}		Proportion of Total Spatial Variation (%)	
		Spatial	Pure Spatial	Spatial	Pure Spatial
T2 (Environmental adversity as a conditional variable)	Broad	0.57	0.53	73.89	70.83
	Medium	0.06	0.06	7.87	8.42
	Fine	0.14	0.16	18.24	20.76
	Total	0.78	0.75	100.00	100.00
Range (Competitive adversity as a conditional variable)	Broad	0.31	0.26	54.00	51.85
	Medium	0.09	0.10	15.18	18.97
	Fine	0.18	0.15	30.83	29.18
	Total	0.57	0.51	100.00	100.00
T4 (Competitive adversity as a conditional variable)	Broad	0.35	0.29	47.21	43.07
	Medium	0.19	0.19	25.78	28.09
	Fine	0.20	0.19	27.02	28.84
	Total	0.74	0.67	100.00	100.00

The scale-specific partitioning revealed distinct patterns among SES metrics (Table 4). For T2, broad-scale spatial variation was dominant, accounting for 73.89% of the total spatially explained variation (70.83% after conditioning on environmental adversity). This pattern indicates a strong association between environmental filtering patterns and broad-scale spatial structures. In contrast, Range and T4 exhibited relatively greater contributions from medium- and fine-scale spatial components, which together accounted for 46.00% and

52.79% of their respective total spatial variation. These results suggest that competition-related patterns are more strongly associated with meso- and fine-scale spatial structures than those captured by T2. Conditioning on the corresponding adversity gradients reduced the total spatially explained variation from 0.777 to 0.753 for T2, from 0.567 to 0.506 for Range, and from 0.737 to 0.670 for T4. The largest absolute reductions were observed for T4 and Range, suggesting that competitive adversity shares part of its spatial structure with the MEM-based predictors. For T2, the reduction was smaller and was primarily associated with the broad-scale component, consistent with the predominantly broad-scale spatial structure of environmental adversity.

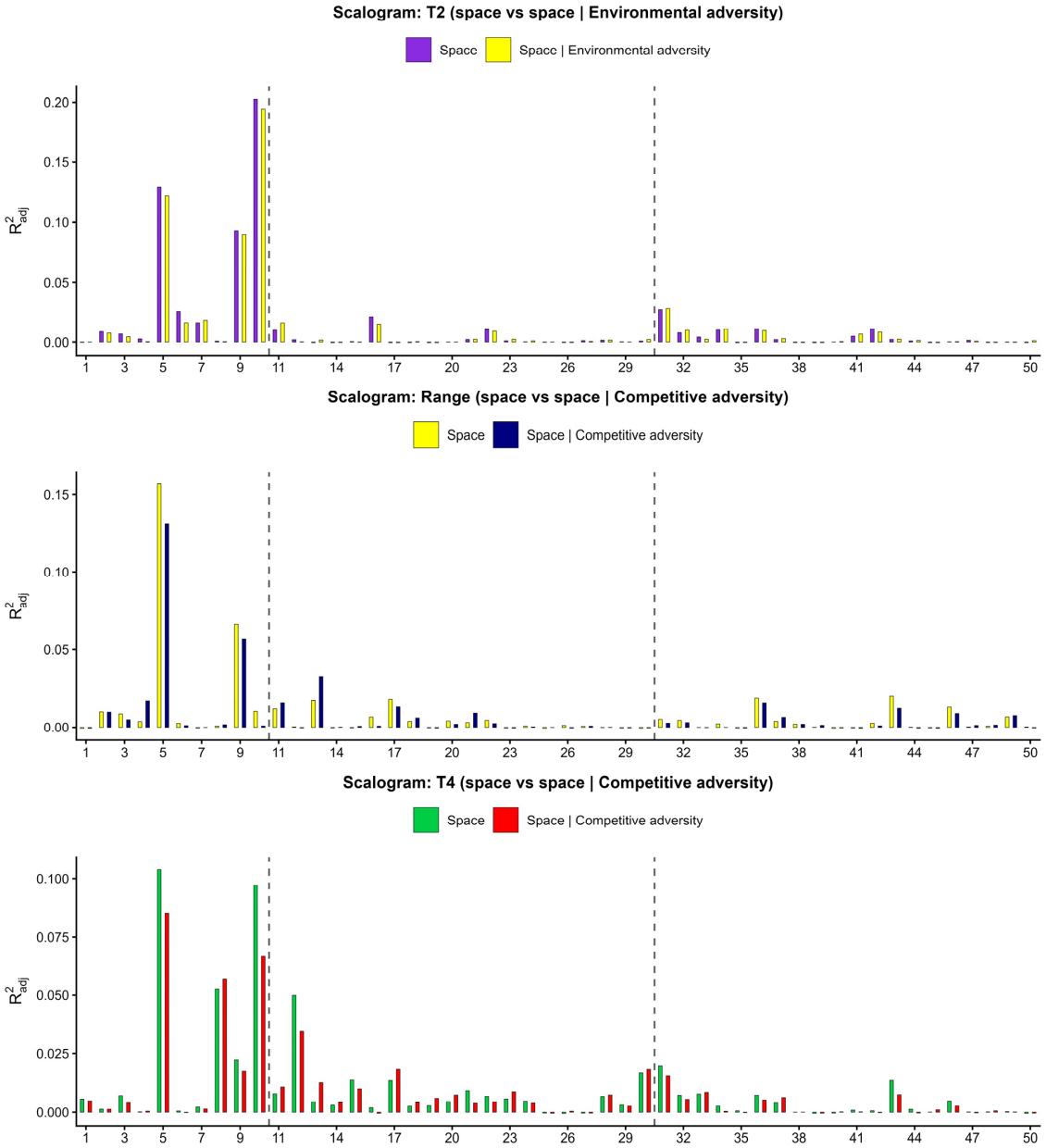


Figure 8. Scalograms of SES variation explained by individual MEM-based spatial predictors, showing the total spatial component ("Space") and the partial spatial component after conditioning on competitive or environmental adversity ("Space|adversity"). Broad-scale spatial variation is represented by MEM variables 1–10, medium-scale variation by MEM variables 11–30, and fine-scale variation by MEM variables 31–485. Vertical dashed lines indicate the boundaries between spatial scale classes. For clarity, only the first 50 MEM variables are displayed, representing the dominant spatial structures.

4. Discussion

4.1. Environmental and Competitive Adversity Gradients

The Stress Dominance Hypothesis (SDH) concept of variation in community assembly rules along both environmental and competitive adversity gradients [13]. This hypothesis represents a logical development of earlier ideas on the habitat templet, in which community organisation is constrained by two fundamental axes reflecting disturbance and environmental adversity [92]. Given the difficulty of directly measuring environmental stress, this hypothesis was further extended by using various ecological gradients, provided that they impose a certain level of stress on the focal taxonomic group [19]. The original formulation of the SDH was revisited in the present study [13], which required considering the indicators of both environmental and competitive adversity. No environmental gradient was *a priori* defined as a stress factor. Instead, the state of environmental stress was inferred from indicators derived from the community itself. These stress indicators can subsequently be interpreted *a posteriori* in relation to the measured characteristics of environmental factors. Obvious markers of environmental adversity are stress-tolerant species, whereas competitive species, according to Grime's framework, serve as markers of competitive adversity [93]. These plant strategies, together with ruderals, are typically expressed as proportions that sum to 1 [59], which makes them compositional variables constrained to the simplex. At local scales, CSR ecological strategies can even outperform individual functional traits in explaining species dominance, highlighting their value as integrative indicators of how plants respond to stress and resource limitation [94]. CSR strategies also provide insights into competitive dynamics within plant communities. The balance among C-, S- and R-strategists reflects the prevailing level of abiotic stress and also the intensity and nature of competition [95].

The Stress–Dominance Hypothesis (SDH), as formulated by Swenson and Enquist [14], applies to any abiotic gradient that elicits a genuinely stress-driven community response. Within this segment of the gradient, the "stressful abiotic environment is the primary determinant of mean trait values and variances", and dominance is conferred by those traits that provide a competitive advantage under stressful conditions, rather than by a relaxation or replacement of competition. Species coexistence requires differences in ecological niches, whereas environmental harshness alone does not create such differences [96]. At the same time, the hypothesis does not require a mirror-image pattern at the less stressful end of the gradient. On the contrary, it explicitly allows for the full spectrum of trait dispersion patterns (clustering, randomness, and overdispersion) as stress decreases. Accordingly, the predictive component of the SDH is strongest within the range in which communities exhibit a stress response. In contrast, outside this zone, multiple context-dependent trajectories of trait structure are possible.

4.2. Trait Matrices Are Separately Sensitive to Environmental Factors and Competition

The Stress Dominance Hypothesis (SDH) also emphasises the sensitivity of traits to either environmental factors or competition [13]. This aspect has been widely considered in empirical studies [32]. The balance between environmental filtering and similarity constraints depends on traits and habitat context: resource-use traits are primarily limited by filtering under harsh conditions, whereas similarity constraints shape regeneration traits and may allow diversity to persist even in stressful environments [32]. The coinciding and opposing effects of environmental filtering and competition may mutually cancel each other out, resulting in an apparently stochastic pattern when traits are analysed without distinguishing their sensitivity to environmental factors and competition.

The residual trait matrix represents the component of the original trait variation remaining after the extraction of the environment-sensitive and competition-sensitive components.

Its substantial inertia indicates that a considerable proportion of trait variation was not assigned to either of these components. Importantly, the residual component exhibited a systematic pattern in the observed communities, suggesting that it should not be regarded simply as statistical noise. This pattern resembled the response expected under asymmetric competition, although the underlying mechanism remains to be established. The residual variation may therefore reflect unmeasured environmental conditions, aspects of competitive interactions not captured by our approach, or other ecological processes. The relative contribution of the components may depend on methodological choices, including the selection of RLQ axes, CCA conditioning, and ridge regularisation. This distinction is particularly important when extending the null-model framework originally developed and tested through numerical simulations [9], where trait sensitivity to environmental filtering or competition can be specified a priori. In empirical communities, such sensitivities are rarely exclusive, and the separation of trait variation into distinct components provides a pragmatic means of identifying their predominant associations while acknowledging the complexity of ecological responses.

4.3. Comparison of the Best-Performing Randomisation Models with Those Obtained from Numerical Modelling

The comparison of numerical predictions and empirical observations reveals different levels of support for the assembly mechanisms underlying the Stress–Dominance Hypothesis. Environmental filtering shows the clearest agreement: the T2 randomisation applied to environment-sensitive traits consistently detects convergence along the environmental adversity gradient. However, significant trait convergence also occurs where measured environmental gradients are weak, suggesting that these traits capture ecological heterogeneity not fully represented by the measured variables. Competition-related divergence is more sensitive to the choice of null model and trait component. Consistent with previous evaluations [9], richness-only randomisations such as C1 have limited sensitivity to limiting similarity, whereas the Range randomisation applied to competition-sensitive traits produces the clearest positive effect sizes. This supports the importance of combining appropriate randomisation procedures with functionally differentiated trait matrices. Evidence for asymmetric competition is less conclusive. Although negative T4 effect sizes indicate trait convergence, this signal weakens at the highest levels of competitive adversity, contrary to theoretical expectations. This discrepancy may reflect the indirect nature of the adversity indicator and the influence of unmeasured ecological processes on residual trait variation. T4 convergence cannot be attributed exclusively to asymmetric competitive exclusion. Environmental filtering and competition-related divergence show relatively strong agreement between numerical predictions and empirical patterns, whereas support for asymmetric competitive exclusion remains limited. These findings demonstrate the importance of distinguishing trait patterns consistent with particular assembly mechanisms from direct evidence of those mechanisms.

4.4. Spatial Scaling of Adversity Gradients Under the Stress–Dominance Hypothesis

Spatial scale is pivotal for discussing the Stress–Dominance Hypothesis (SDH) in the context of this problem. Grime [6] traces the study of how competition shapes community structure back to Darwin, and the study of environmental controls back to the classic plant geographers, thereby implicitly delineating the spatial domains over which competitive processes and environmental drivers predominantly operate. Because these domains differ substantially, competitive adversity cannot be expected to coincide with environmental adversity: the two axes are associated with different spatial scales of ecological variation. Our results indicate that, fully consistent with SDH, environmental filtering produces

broad-scale spatial patterns, whereas interspecific competition is expressed more strongly at intermediate or fine spatial scales. This interpretation accords with evidence that inferred mechanisms of community assembly can shift markedly with spatial scale, with environmental filtering emerging at broader scales and competitive interactions becoming detectable only at finer neighbourhood scales [97,98]. Environmental filtering exhibits broad-scale spatial patterning in indices of richness and dominance. In contrast, biotic interactions generate small-scale signatures of spatial autocorrelation, mainly in indices of plant community diversity [98]. Competition-associated effects on functional traits are expected to be most detectable at fine spatial scales, where interacting plants occur in close proximity or have overlapping resource-use zones within relatively homogeneous communities. In contrast, broad spatial scales facilitate the detection of systematic environmental gradients, whose effects on functional traits may be obscured at finer scales by local heterogeneity and stochastic variation. Medium scales represent a transition where both types of effects may be detectable. In heterogeneous floodplain landscapes, however, the spatial extent of relatively homogeneous communities and environmental gradients can vary considerably.

It is important to distinguish the statistical spatial scales identified by Moran's eigenvector maps (MEM) from the spatial grain of field sampling. MEM-based broad-, medium-, and fine-scale components describe patterns of spatial variation relative to the configuration and extent of the sampling network, rather than directly corresponding to particular physical distances or ecological processes. The predominance of a given MEM scale should not be interpreted as direct evidence that a specific community assembly mechanism operates at that scale. Similar spatial patterns may arise from different ecological processes, while individual processes may generate variation across multiple spatial scales. Our results therefore characterise the spatial organisation of trait assembly patterns rather than providing a direct spatial attribution of the mechanisms responsible for them.

4.5. Study Limitations and Implications

The principal limitation of this study concerns the quantification of interspecific competition, which remains a major methodological challenge in community ecology. This issue is particularly important for our approach, as the identification of competition-sensitive trait variation depends on the reliability of competition estimates. If independently validated, the proposed approach could provide an efficient tool for assessing multiple competitive interactions across ecological communities. Otherwise, alternative methods of competition assessment will need to be explored. Further limitations concern the characterisation of functional traits and environmental conditions. Trait values should be region-specific to better reflect local ecological adaptations and phenotypic variability. The inclusion of additional physiological and biochemical traits, particularly indicators of photosynthetic performance and pigment composition, could provide a more comprehensive characterisation of plant responses. Environmental measurements could be expanded to include more direct indicators of nutrient availability and eutrophication, allowing a more detailed assessment of environmental filtering. Addressing these limitations would improve the reliability, ecological interpretation, and broader applicability of the proposed framework.

The proposed framework may also be applicable beyond vascular plant communities, as the distinction between environmental filtering and biotic interactions is relevant to a wide range of organisms. Its application to non-vascular taxa would require appropriate functional traits and methods for quantifying interactions, whereas mobile organisms would additionally require consideration of movement, spatial overlap, and the temporal variability of interactions. Although the general principle of separating environment-associated and competition-associated trait variation is potentially transferable across taxa, its practical implementation and reliability require independent validation for each ecological context.

5. Conclusions

An empirical framework for testing the Stress–Dominance Hypothesis (SDH) was developed by explicitly addressing three fundamental aspects of community assembly. Environmental and competitive adversity were treated as two distinct dimensions rather than opposite ends of a single stress gradient. Trait-matrix decomposition accounted for the fact that classifying functional traits as exclusively environment-sensitive or competition-sensitive is an oversimplification, since their responses may reflect multiple ecological processes. Spatial-scale analysis recognised that community assembly mechanisms operate within spatially structured environments and that their effects may differ across spatial scales. The empirical results supported the importance of these distinctions. Environmental adversity was associated with trait convergence and predominantly broad-scale spatial variation, consistent with environmental filtering. Competitive adversity was associated with both trait divergence and convergence, potentially reflecting symmetric and asymmetric competitive processes, respectively, and exhibited a more heterogeneous spatial structure. The substantial residual trait variation further indicated that community assembly cannot be fully characterised by environmental and competitive sensitivity alone. These findings demonstrate that accounting for distinct adversity gradients, overlapping trait sensitivities, and spatial scale provides a more comprehensive basis for testing SDH predictions and interpreting functional community assembly in empirical ecosystems.

Supplementary Materials: The following supporting information can be downloaded at: https://www.mdpi.com/article/10.3390/d18110711/s1. Table S1: Fixed effects of the Gaussian GLMM for environmental and competitive adversities (N = 1812 observations in 453 sites); Table S2: Proportion of trait variation explained by environmental factors, competitive interactions, and unexplained (residual) variance; Table S3: Power analysis and simulated effect sizes for alternative community assembly scenarios across trait blocks: Power = proportion of significant detections; Prop ± SD = mean proportional effect ± standard deviation; SES = standardized effect size relative to null expectations; Table S4: Model performance of hierarchical generalized additive models (HGAMs) describing the relationships between effect sizes (Range, T4, and T2) and competitive or environmental adversity gradients across waterbody types. G denotes a global smooth model; GS denotes a model combining a global smooth with waterbody-type-specific smooth deviations; and S denotes a model with waterbody-type-specific smooths only. Model performance was evaluated using the corrected Akaike information criterion (AICc), adjusted coefficient of determination (Adj. R^2), and percentage of deviance explained. Lower AICc values indicate better model support. All models were fitted using maximum likelihood (ML; n = 1,812 observations for each response variable); Figure S1: Effect sizes from plot-level trait convergence/divergence tests along competitive (Range, T4) and environmental (T2) adversity gradients across months (V–VIII). Points are plot-level effect sizes; black solid lines and grey ribbons show fitted curves and 95% confidence intervals from the GT model (global + month-specific smooths), whereas red dashed lines depict the global G model.

Author Contributions: Conceptualisation, J.-C.S. and O.Z.; methodology, O.L.; software, O.K.; validation, A.Z., H.T. and O.K.; formal analysis, O.Z.; investigation, H.T.; resources, O.Z.; data curation, O.L.; writing—original draft preparation, O.Z.; writing—review and editing, J.-C.S.; visualisation, O.Z.; supervision, O.K.; project administration, A.Z.; funding acquisition, O.Z. All authors have read and agreed to the published version of the manuscript.

Funding: SARU grant (Fellowship for Scholars at Risk from Ukrainian Universities), which enabled her to continue scientific research in a safe environment during wartime. JCS was supported by Center for Ecological Dynamics in a Novel Biosphere (ECONOVO), funded by Danish National Research Foundation (grant DNRF173). This research was funded by National Research Foundation of Ukraine, grant number 2025.07/0001 "Procrustean analysis of spectral indices for assessing changes in hemeroby and the functional structure of plant communities as a result of military destruction: the example of the destruction of the Kakhovka Reservoir".

Institutional Review Board Statement: Not applicable. Ethical approval was not required for this study, as it did not involve humans or animals.

Data Availability Statement: The data supporting the results of this study are publicly available via GBIF as an occurrence dataset [99].

Acknowledgments: The authors thank the staff of the Dnipro-Orilskiy Nature Reserve for facilitating the research and providing logistical support. They also appreciate the Armed Forces of Ukraine for ensuring their security and for their unwavering commitment to freedom and independence.

Conflicts of Interest: The authors declare no conflicts of interest.

References

1. Mouchet, M.A.; Villéger, S.; Mason, N.W.H.; Mouillot, D. Functional Diversity Measures: An Overview of Their Redundancy and Their Ability to Discriminate Community Assembly Rules. *Funct. Ecol.* **2010**, *24*, 867–876. [CrossRef]
2. Keddy, P.A. Assembly and Response Rules: Two Goals for Predictive Community Ecology. *J. Veg. Sci.* **1992**, *3*, 157–164. [CrossRef]
3. Perronne, R.; Munoz, F.; Borgy, B.; Reboud, X.; Gaba, S. How to Design Trait-Based Analyses of Community Assembly Mechanisms: Insights and Guidelines from a Literature Review. *Perspect. Plant Ecol. Evol. Syst.* **2017**, *25*, 29–44. [CrossRef]
4. Macarthur, R.; Levins, R. The Limiting Similarity, Convergence, and Divergence of Coexisting Species. *Am. Nat.* **1967**, *101*, 377–385. [CrossRef]
5. Case, T.J.; Sidell, R. Pattern and Chance in the Structure of Model and Natural Communities. *Evolution* **1983**, *37*, 832–849. [CrossRef] [PubMed]
6. Grime, J.P. Trait Convergence and Trait Divergence in Herbaceous Plant Communities: Mechanisms and Consequences. *J. Veg. Sci.* **2006**, *17*, 255–260. [CrossRef]
7. Mayfield, M.M.; Levine, J.M. Opposing Effects of Competitive Exclusion on the Phylogenetic Structure of Communities. *Ecol. Lett.* **2010**, *13*, 1085–1093. [CrossRef]
8. Grime, J.P. Competitive Exclusion in Herbaceous Vegetation. *Nature* **1973**, *242*, 344–347. [CrossRef]
9. Götzenberger, L.; Botta-Dukát, Z.; Lepš, J.; Pärtel, M.; Zobel, M.; de Bello, F. Which Randomizations Detect Convergence and Divergence in Trait-based Community Assembly? A Test of Commonly Used Null Models. *J. Veg. Sci.* **2016**, *27*, 1275–1287. [CrossRef]
10. Götzenberger, L.; de Bello, F.; Bråthen, K.A.; Davison, J.; Dubuis, A.; Guisan, A.; Lepš, J.; Lindborg, R.; Moora, M.; Pärtel, M.; et al. Ecological Assembly Rules in Plant Communities—Approaches, Patterns and Prospects. *Biol. Rev.* **2012**, *87*, 111–127. [CrossRef]
11. Jin, L.S.; Yin, D.; Fortin, M.-J.; Cadotte, M.W. The Mechanisms Generating Community Phylogenetic Patterns Change with Spatial Scale. *Oecologia* **2020**, *193*, 655–664. [CrossRef] [PubMed]
12. Münkemüller, T.; Gallien, L.; Lavergne, S.; Renaud, J.; Roquet, C.; Abdulhak, S.; Dullinger, S.; Garraud, L.; Guisan, A.; Lenoir, J.; et al. Scale Decisions Can Reverse Conclusions on Community Assembly Processes. *Glob. Ecol. Biogeogr.* **2014**, *23*, 620–632. [CrossRef] [PubMed]
13. Weiher, E.; Keddy, P.A. Assembly Rules, Null Models, and Trait Dispersion: New Questions from Old Patterns. *Oikos* **1995**, *74*, 159. [CrossRef]
14. Swenson, N.G.; Enquist, B.J. Ecological and Evolutionary Determinants of a Key Plant Functional Trait: Wood Density and Its Community-wide Variation across Latitude and Elevation. *Am. J. Bot.* **2007**, *94*, 451–459. [CrossRef] [PubMed]
15. Grime, J.P. The Stress Debate: Symptom of Impending Synthesis? *Biol. J. Linn. Soc.* **1989**, *37*, 3–17. [CrossRef]
16. Drake, J.A. Community-Assembly Mechanics and the Structure of an Experimental Species Ensemble. *Am. Nat.* **1991**, *137*, 1–26. [CrossRef]
17. Pakgohar, N.; Barabás, S.; Ćuk, M.; Csecserits, A.; Gyalus, A.; Lengyel, A.; Lhotsky, B.; Mártonffy, A.; Ónodi, G.; Rédei, T.; et al. Low Replicability of Testing the Stress–Dominance Hypothesis Using a Trait Convergence/Divergence Pattern. *J. Veg. Sci.* **2024**, *35*, e13260. [CrossRef]
18. Coyle, J.R.; Halliday, F.W.; Lopez, B.E.; Palmquist, K.A.; Wilfahrt, P.A.; Hurlbert, A.H. Using Trait and Phylogenetic Diversity to Evaluate the Generality of the Stress-dominance Hypothesis in Eastern North American Tree Communities. *Ecography* **2014**, *37*, 814–826. [CrossRef]
19. Lopez, B.; Burgio, K.; Carlucci, M.; Palmquist, K.; Parada, A.; Weinberger, V.; Hurlbert, A. A New Framework for Inferring Community Assembly Processes Using Phylogenetic Information, Relevant Traits and Environmental Gradients. *One Ecosyst.* **2016**, *1*, e9501. [CrossRef]
20. Pickett, S.T.A.; Bazzaz, F.A. Organization of Anassemblage of Early Successional Species on a Soil Moisture Gradient. *Ecology* **1978**, *59*, 1248–1255. [CrossRef]

21. Jiang, Y.; Chen, Z.; Lin, H.; Deng, R.; Liang, Z.; Li, Y.; Liang, S. Trait-Based Community Assembly and Functional Strategies across Three Subtropical Karst Forests, Southwestern China. *Front. Plant Sci.* **2024**, *15*, 1451981. [CrossRef] [PubMed]
22. Douma, J.C.; Shipley, B.; Witte, J.-P.M.; Aerts, R.; van Bodegom, P.M. Disturbance and Resource Availability Act Differently on the Same Suite of Plant Traits: Revisiting Assembly Hypotheses. *Ecology* **2012**, *93*, 825–835. [CrossRef]
23. Carscadden, K.A.; Cadotte, M.W.; Gilbert, B. Trait Dimensionality and Population Choice Alter Estimates of Phenotypic Dissimilarity. *Ecol. Evol.* **2017**, *7*, 2273–2285. [CrossRef] [PubMed]
24. Argyle, P.A.; Walworth, N.G.; Hinners, J.; Collins, S.; Levine, N.M.; Doblin, M.A. Multivariate Trait Analysis Reveals Diatom Plasticity Constrained to a Reduced Set of Biological Axes. *ISME Commun.* **2021**, *1*, 59. [CrossRef] [PubMed]
25. Ingram, T.; Shurin, J.B. Trait-based Assembly and Phylogenetic Structure in Northeast Pacific Rockfish Assemblages. *Ecology* **2009**, *90*, 2444–2453. [CrossRef]
26. Valverde-Barrantes, O.J.; Lugli, L.F.; Fuchslueger, L.; Hofhansl, F.; Martins, N.; Cordeiro, A.L.; Schapp, K.; Anderson, K.M.; Garcia, S.; Grandis, A.; et al. Rainfall Seasonality Shapes Belowground Root Trait Dynamics in an Amazonian Tropical Rainforest: A Test of the Stress-dominance Hypothesis. *Funct. Ecol.* **2025**, *39*, 799–812. [CrossRef]
27. Ács, É.; Földi, A.; Vad, C.F.; Trábert, Z.; Kiss, K.T.; Duleba, M.; Borics, G.; Grigorszky, I.; Botta-Dukát, Z. Trait-Based Community Assembly of Epiphytic Diatoms in Saline Astatic Ponds: A Test of the Stress-Dominance Hypothesis. *Sci. Rep.* **2019**, *9*, 15749. [CrossRef]
28. Gafta, D.; Oroian, S.; Sămărghițan, M. Community Level Trait Patterns Are Detectable Even along Short Stress Gradients but Not Readily Predictable under Very Limited Soil Resources. *Sci. Rep.* **2025**, *15*, 36608. [CrossRef]
29. Cornwell, W.K.; Ackerly, D.D. Community Assembly and Shifts in Plant Trait Distributions across an Environmental Gradient in Coastal California. *Ecol. Monogr.* **2009**, *79*, 109–126. [CrossRef]
30. Spasojevic, M.J.; Suding, K.N. Inferring Community Assembly Mechanisms from Functional Diversity Patterns: The Importance of Multiple Assembly Processes. *J. Ecol.* **2012**, *100*, 652–661. [CrossRef]
31. Gross, N.; Börger, L.; Soriano-Morales, S.I.; Le Bagousse-Pinguet, Y.; Quero, J.L.; García-Gómez, M.; Valencia-Gómez, E.; Maestre, F.T. Uncovering Multiscale Effects of Aridity and Biotic Interactions on the Functional Structure of Mediterranean Shrublands. *J. Ecol.* **2013**, *101*, 637–649. [CrossRef]
32. Lhotsky, B.; Kovács, B.; Ónodi, G.; Csecserits, A.; Rédei, T.; Lengyel, A.; Kertész, M.; Botta-Dukát, Z. Changes in Assembly Rules along a Stress Gradient from Open Dry Grasslands to Wetlands. *J. Ecol.* **2016**, *104*, 507–517. [CrossRef]
33. Botta-Dukát, Z.; Czúcz, B. Testing the Ability of Functional Diversity Indices to Detect Trait Convergence and Divergence Using Individual-based Simulation. *Methods Ecol. Evol.* **2016**, *7*, 114–126. [CrossRef]
34. Backhaus, L.; Albert, G.; Cuchietti, A.; Jaimes Nino, L.M.; Fahs, N.; Lisner, A.; Kolář, V.; Kermavnar, J.; Widmer, S.; Zimmermann, Z.; et al. Shift from Trait Convergence to Divergence along Old-field Succession. *J. Veg. Sci.* **2021**, *32*, e12986. [CrossRef]
35. Ran, Y.; Wu, S.; Chen, C.; Sun, X.; Huang, P.; Ma, M.; Yi, X. Shift from Soil Chemical to Physical Filters in Assembling Riparian Floristic Communities along a Flooding Stress Gradient. *Sci. Total Environ.* **2022**, *844*, 157116. [CrossRef] [PubMed]
36. Selye, H. Stress and the General Adaptation Syndrome. *BMJ* **1950**, *1*, 1383–1392. [CrossRef]
37. Selye, H. *The Stress of Life*; McGraw-Hill: New York, NY, USA, 1956; ISBN 0070562067.
38. Körner, C. Limitation and Stress—Always or Never? *J. Veg. Sci.* **2003**, *14*, 141–143. [CrossRef]
39. Choler, P.; Michalet, R.; Callaway, R.M. Facilitation and Competition on Gradients in Alpine Plant Communities. *Ecology* **2001**, *82*, 3295. [CrossRef]
40. Liancourt, P.; Callaway, R.M.; Michalet, R. Stress Tolerance and Competitive-Response Ability Determine the Outcome of Biotic Interactions. *Ecology* **2005**, *86*, 1611–1618. [CrossRef]
41. Maestre, F.T.; Callaway, R.M.; Valladares, F.; Lortie, C.J. Refining the Stress-gradient Hypothesis for Competition and Facilitation in Plant Communities. *J. Ecol.* **2009**, *97*, 199–205. [CrossRef]
42. Hunt, R.; Hodgson, J.G.; Thompson, K.; Bungener, P.; Dunnett, N.; Askew, A. A New Practical Tool for Deriving a Functional Signature for Herbaceous Vegetation. *Appl. Veg. Sci.* **2004**, *7*, 163–170. [CrossRef]
43. Ferré, C.; Caccianiga, M.; Zanzottera, M.; Comolli, R. Soil–Plant Interactions in a Pasture of the Italian Alps. *J. Plant Interact.* **2020**, *15*, 39–49. [CrossRef]
44. Bonari, G.; Padullés Cubino, J.; Sarmati, S.; Landi, M.; Zerbe, S.; Marcenò, C.; Scoppola, A.; Angiolini, C. Ecosystem State Assessment after More than 100 Years since Planting for Dune Consolidation. *Restor. Ecol.* **2021**, *29*, e13435. [CrossRef]
45. Mastrogianni, A.; Kiziridis, D.A.; Karadimou, E.; Pleniou, M.; Xystrakis, F.; Tsiftsis, S.; Tsiripidis, I. Community-Level Differentiation of Grime's CSR Strategies along a Post-Abandonment Secondary Successional Gradient. *Flora* **2023**, *308*, 152399. [CrossRef]
46. Conti, L.; de Bello, F.; Lepš, J.; Acosta, A.T.R.; Carboni, M. Environmental Gradients and Micro-heterogeneity Shape Fine-scale Plant Community Assembly on Coastal Dunes. *J. Veg. Sci.* **2017**, *28*, 762–773. [CrossRef]

47. Dullinger, S.; Kleinbauer, I.; Pauli, H.; Gottfried, M.; Brooker, R.; Nagy, L.; Theurillat, J.-P.; Holten, J.I.; Abdaladze, O.; Benito, J.-L.; et al. Weak and Variable Relationships between Environmental Severity and Small-scale Co-occurrence in Alpine Plant Communities. *J. Ecol.* **2007**, *95*, 1284–1295. [CrossRef]
48. de Bello, F.; Vandewalle, M.; Reitalu, T.; Lepš, J.; Prentice, H.C.; Lavorel, S.; Sykes, M.T. Evidence for Scale- and Disturbance-dependent Trait Assembly Patterns in Dry Semi-natural Grasslands. *J. Ecol.* **2013**, *101*, 1237–1244. [CrossRef]
49. Rao, C.R. Diversity and Dissimilarity Coefficients: A Unified Approach. *Theor. Popul. Biol.* **1982**, *21*, 24–43. [CrossRef]
50. Tutova, H.; Lisovets, O.; Kunakh, O.; Zymaroieva, A.; Svenning, J.-C.; Zhukov, O. *R Code and Data for Null-Model Randomization and Competition Analysis in Aquatic Macrophyte Communities [Dataset]*; Zenodo: Meyrin, Switzerland, 2026. [CrossRef]
51. Dolédec, S.; Chessel, D.; Ter Braak, C.J.F.; Champely, S. Matching Species Traits to Environmental Variables: A New Three-Table Ordination Method. *Environ. Ecol. Stat.* **1996**, *3*, 143–166. [CrossRef]
52. Dray, S.; Dufour, A.B. The Ade4 Package: Implementing the Duality Diagram for Ecologists. *J. Stat. Softw.* **2007**, *22*, 1–20. [CrossRef]
53. Ter Braak, C.J.F. Canonical Correspondence Analysis: A New Eigenvector Technique for Multivariate Direct Gradient Analysis. *Ecology* **1986**, *67*, 1167–1179. [CrossRef]
54. García-Callejas, D.; Godoy, O.; Bartomeus, I. Cxr: A Toolbox for Modelling Species Coexistence in R. *Methods Ecol. Evol.* **2020**, *11*, 1221–1226. [CrossRef]
55. Golub, G.H.; Reinsch, C. Singular Value Decomposition and Least Squares Solutions. *Numer. Math.* **1970**, *14*, 403–420. [CrossRef]
56. ter Braak, C.J.F.; Cormont, A.; Dray, S. Improved Testing of Species Traits–Environment Relationships in the Fourth-corner Problem. *Ecology* **2012**, *93*, 1525–1526. [CrossRef] [PubMed]
57. Bernhardt-Römermann, M.; Römermann, C.; Nuske, R.; Parth, A.; Klotz, S.; Schmidt, W.; Stadler, J. On the Identification of the Most Suitable Traits for Plant Functional Trait Analyses. *Oikos* **2008**, *117*, 1533–1541. [CrossRef]
58. Hoerl, A.E.; Kennard, R.W. Ridge Regression: Biased Estimation for Nonorthogonal Problems. *Technometrics* **1970**, *12*, 55–67. [CrossRef]
59. Pierce, S.; Negreiros, D.; Cerabolini, B.E.L.; Kattge, J.; Díaz, S.; Kleyer, M.; Shipley, B.; Wright, S.J.; Soudzilovskaia, N.A.; Onipchenko, V.G.; et al. A Global Method for Calculating Plant Ecological Strategies Applied across Biomes World-wide. *Funct. Ecol.* **2017**, *31*, 444–457. [CrossRef]
60. Egozcue, J.J.; Pawlowsky-Glahn, V.; Mateu-Figueras, G.; Barceló-Vidal, C. Isometric Logratio Transformations for Compositional Data Analysis. *Math. Geol.* **2003**, *35*, 279–300. [CrossRef]
61. Pedersen, E.J.; Miller, D.L.; Simpson, G.L.; Ross, N. Hierarchical Generalized Additive Models in Ecology: An Introduction with Mgcv. *PeerJ* **2019**, *7*, e6876. [CrossRef] [PubMed]
62. Zuur, A.F.; Ieno, E.N.; Walker, N.J.; Saveliev, A.A.; Smith, G.M. Generalised Estimation Equations. In *Mixed effects models and extensions in ecology with R. Statistics for Biology and Health*; Gail, M., Krickeberg, K., Samet, J.M., Tsiatis, A., Wong, W., Eds.; Springer: New York, NY, USA, 2009; pp. 295–321.
63. Tutova, H.; Lisovets, O.; Kunakh, O.; Zymaroieva, A.; Svenning, J.-C.; Zhukov, O. *Data and R Code for Testing the Stress–Dominance Hypothesis in Aquatic Macrophyte Communities Using Hierarchical Generalized Additive Models [Dataset]*; Zenodo: Meyrin, Switzerland, 2026. [CrossRef]
64. Kruskal, J.B. Multidimensional Scaling by Optimizing Goodness of Fit to a Nonmetric Hypothesis. *Psychometrika* **1964**, *29*, 1–27. [CrossRef]
65. Anderson, M.J. A New Method for Non-Parametric Multivariate Analysis of Variance. *Austral Ecol.* **2001**, *26*, 32–46. [CrossRef]
66. Oksanen, J.; Blanchet, F.G.; Friendly, M.; Kindt, R.; Legendre, P.; McGlinn, D.; Minchin, P.R.; O'Hara, R.B.; Simpson, G.L.; Solymos, P.; et al. *Vegan: Community Ecology Package*; R Package Version 2.5-6; CRAN: Vienna, Austria, 2019; Available online: https://CRAN.R-project.org/package=vegan (accessed on 15 November 2026).
67. Vislocky, R.L.; Fritsch, J.M.; Vislocky, R.L.; Fritsch, J.M. Generalized Additive Models versus Linear Regression in Generating Probabilistic MOS Forecasts of Aviation Weather Parameters. *Weather Forecast.* **1995**, *10*, 669–680. [CrossRef]
68. Blanchet, F.G.; Legendre, P.; Borcard, D. Modelling Directional Spatial Processes in Ecological Data. *Ecol. Modell.* **2008**, *215*, 325–336. [CrossRef]
69. Legendre, P.; Gauthier, O. Statistical Methods for Temporal and Space-Time Analysis of Community Composition Data. *Proc. R. Soc. B Biol. Sci.* **2014**, *281*, 20132728. [CrossRef] [PubMed]
70. Dray, S.; Legendre, P.; Peres-Neto, P.R. Spatial Modelling: A Comprehensive Framework for Principal Coordinate Analysis of Neighbour Matrices (PCNM). *Ecol. Modell.* **2006**, *196*, 483–493. [CrossRef]
71. Griffith, D.A.; Peres-Neto, P.R. Spatial Modeling in Ecology: The Flexibility of Eigenfunction Spatial Analyses. *Ecology* **2006**, *87*, 2603–2613. [CrossRef]
72. R Core Team. *R: A Language and Environment for Statistical Computing*; R Core Team: Vienna, Austria, 2025.
73. Oksanen, J.; Blanchet, F.G.; Kindt, R.; Legendre, P.; Minchin, P.R.; O'Hara, R.B.; Simpson, G.L.; Solymos, P.; Stevens, M.H.H.; Wagner, H. *Community Ecology Package*; R Package Version 2.5-2; CRAN: Vienna, Austria, 2018.

74. Dray, S.; Bauman, D.; Blanchet, G.; Borcard, D.; Clappe, S.; Guenard, G.; Jombart, T.; Larocque, G.; Legendre, P.; Madi, N.; et al. *Adespatial: Multivariate Multiscale Spatial Analysis*; R Package Version 0.3-2; CRAN: Vienna, Austria, 2018.
75. Anselin, L. *Spatial Regression Analysis in R–A Workbook*; University of Illinois at Urbana-Champaign: Urbana, IL, USA, 2005; p. 90.
76. Thioulouse, J.; Dray, S.; Dufour, A.-B.; Siberchicot, A.; Jombart, T.; Pavoine, S. *Multivariate Analysis of Ecological Data with Ade4*; Springer: New York, NY, USA, 2018.
77. Kunakh, O.; Lisovets, O.; Zhukov, O. Hemeroby and Naturalness Differ in Spatial Patterns: The Case of Aquatic Macrophytes. *Int. J. Environ. Stud.* **2024**, *81*, 2692–2706. [CrossRef]
78. Dawidek, J.; Ferencz, B. Hydrochemical Classification of the River Lakes Situated near the Bug River. *Limnol. Rev.* **2005**, *6*, 53–59.
79. Lisovets, O.; Ruchiy, V.; Kunakh, O.; Zhukov, O. The Morphological and Functional Traits of Water Bodies Enhance the Explanatory Power of Directed Spatial Processes in Predicting the Variation of Macrophyte Communities under the Conditions of River Flow Regulation. *River Res. Appl.* **2024**, *40*, 2050–2068. [CrossRef]
80. Tutova, H.; Ruchiy, V.; Khrystov, O.; Lisovets, O.; Kunakh, O.; Zhukov, O. Influence of Morphology and Functional Properties of Floodplain Water Bodies on Species Diversity of Macrophyte Communities. *Regul. Mech. Biosyst.* **2025**, *33*, e25012. [CrossRef]
81. Ruchiy, V.; Khrystov, O.; Kunakh, O.; Zhukov, O. Morphological and Functional Diversity of Floodplain Water Bodies and Their Classification According to the Structure of the Surrounding Vegetation Cover. *Biosyst. Divers.* **2024**, *32*, 60–72. [CrossRef]
82. Hollister, J.; Stachelek, J. Lakemorpho: Calculating Lake Morphometry Metrics in R. *F1000Research* **2017**, *6*, 1718. [CrossRef] [PubMed]
83. Secchi, A. Esperimente per Determinare La Transparenza Del Mare [Experiment to Determine the Transparency of the Sea]. In *On the Wavy Motion of the Sea and on the Currents of it Especially on Those Littoral Ones*; Ciadi, A., Ed.; Tipographia Delle Belle Arti: Rome, Italy, 1866; pp. 258–288.
84. Kattge, J.; Bönisch, G.; Díaz, S.; Lavorel, S.; Prentice, I.C.; Leadley, P.; Tautenhahn, S.; Werner, G.D.A.; Aakala, T.; Abedi, M.; et al. TRY Plant Trait Database—Enhanced Coverage and Open Access. *Glob. Change Biol.* **2020**, *26*, 119–188. [CrossRef] [PubMed]
85. Raunkiaer, C. *Plant Life Forms*; Clarendon Press: Oxford, UK, 1937.
86. Zhukov, O.; Lisovets, O.; Molozhon, K. Differential Ecomorphic Analysis of Urban Park Vegetation. *IOP Conf. Ser. Earth Environ. Sci.* **2023**, *1254*, 012023. [CrossRef]
87. Tarasov, V.V. *Flora of Dnipropetrovsk and Zaporizhia Regions*; Travleev, A.P., Ed.; Lira: Dnipropetrovsk, Ukraine, 2012. (In Ukranian)
88. Willby, N.J.; Abernethy, V.J.; Demars, B.O.L. Attribute-based Classification of European Hydrophytes and Its Relationship to Habitat Utilization. *Freshw. Biol.* **2000**, *43*, 43–74. [CrossRef] [PubMed]
89. Lososová, Z.; Axmanová, I.; Chytrý, M.; Midolo, G.; Abdulhak, S.; Karger, D.N.; Renaud, J.; Van Es, J.; Vittoz, P.; Thuiller, W. Seed Dispersal Distance Classes and Dispersal Modes for the European Flora. *Glob. Ecol. Biogeogr.* **2023**, *32*, 1485–1494. [CrossRef]
90. Tichý, L.; Axmanová, I.; Dengler, J.; Guarino, R.; Jansen, F.; Midolo, G.; Nobis, M.P.; Van Meerbeek, K.; Aćić, S.; Attorre, F.; et al. Ellenberg-type Indicator Values for European Vascular Plant Species. *J. Veg. Sci.* **2023**, *34*, e13168. [CrossRef]
91. Tutova, H.; Lisovets, O.; Kunakh, O.; Zymaroieva, A.; Svenning, J.-C.; Zhukov, O. *Functional Trait Dataset of Aquatic Macrophytes from the Dnipro–Orilskyi Nature Reserve, Ukraine [Dataset]*; Zenodo: Meyrin, Switzerland, 2026. [CrossRef]
92. Southwood, T.R.E. Tactics, Strategies and Templets. *Oikos* **1988**, *52*, 3. [CrossRef]
93. Grime, J.P. Evidence for the Existence of Three Primary Strategies in Plants and Its Relevance to Ecological and Evolutionary Theory. *Am. Nat.* **1977**, *111*, 1169–1194. [CrossRef]
94. Rosado, B.H.P.; de Mattos, E.A. On the Relative Importance of CSR Ecological Strategies and Integrative Traits to Explain Species Dominance at Local Scales. *Funct. Ecol.* **2017**, *31*, 1969–1974. [CrossRef]
95. Navas, M.; Violle, C. Plant Traits Related to Competition: How Do They Shape the Functional Diversity of Communities? *Community Ecol.* **2009**, *10*, 131–137. [CrossRef]
96. Chesson, P.; Huntly, N. The Roles of Harsh and Fluctuating Conditions in the Dynamics of Ecological Communities. *Am. Nat.* **1997**, *150*, 519–553. [CrossRef] [PubMed]
97. Kraft, N.; Ackerly, D. Functional Trait and Phylogenetic Tests of Community Assembly across Spatial Scales in an Amazonian Forest. *Ecol. Monogr.* **2010**, *80*, 401–422. [CrossRef]
98. Lozada, A.; Bertin, A. Spatial Autocorrelation Signatures of Ecological Determinants on Plant Community Characteristics in High Andean Wetlands. *Sci. Rep.* **2022**, *12*, 13770. [CrossRef] [PubMed]
99. Tutova, H.; Ruchiy, V.; Kunakh, O.; Zhukov, O.; Lisovets, O. Macrophyte Species Occurrences in Floodplain Water Bodies of the Dnipro-Orilskyi Nature Reserve, Ukraine (2024). Version 1.9. Bohdan Khmelnytsky Melitopol State Pedagogical University. Occurrence Dataset. 2025. Available online: https://doi.org/10.15468/p3d2rh (accessed on 6 May 2025).

Disclaimer/Publisher's Note: The statements, opinions and data contained in all publications are solely those of the individual author(s) and contributor(s) and not of MDPI and/or the editor(s). MDPI and/or the editor(s) disclaim responsibility for any injury to people or property resulting from any ideas, methods, instructions or products referred to in the content.